ИНСТИТУТ ТЕХНИЧКИХ НАУКА САНУ

Кнез Михаилова 35/IV

11000 Београд, Србија

Предмет: Захтев за покретање поступка за реизбор Адриане Пелеш, дипл. физичара, истраживача сарадника у звање истраживача сарадника

НАУЧНОМ ВЕЋУ ИНСТИТУТА ТЕХНИЧКИХ НАУКА САНУ

Молим Вас да, у складу са Правилником о поступку и начину вредновања, и квантитативном исказивању научноистраживачких резултата истраживача (Сл. Гласник РС, бр.38/08), и Правилником о стицању звања истраживача сарадника, научно веће Института техничких наука САНУ покрене поступак за мој реизбор у звање истраживач сарадник.

За чланове комисије за припрему извештаја Научном Већу предлажем:

- проф. др Владимира Павловића, научног саветника Института техничких наука САНУ
- др Нину Обрадовић, вишег научног сарадника Института техничких наука САНУ
- др Лидију Манчић, научног саветника Института техничких наука САНУ

У прилогу достављам:

1. биографију
2. библиографију са копијом рада
3. доказ о укупној просечној оцени на основним студијама
4. доказ о уписаним докторским студијама

У Београду, 07. 03. 2016.

Подносилац захтева

Адриана Пелеш

Адриана Пелеш, дипл физичар,

истраживач сарадник Института Техничких Наука САНУ

Биографија Адриане Пелеш

Адриана Пелеш рођена је 01. 08. 1984. године у Београду. Дипломирала је на Физичком факултету Универзитета у Београду са просечном оценом 8,2 и 10 на дипломском раду "Коришћење дигиталне видео камере у спектроскопији-калибрација и примена". Постдипломске докторске студије је уписала 2011. године на матичном факулету, смер примењена и компјутерска физика. Тренутно је на трећој години студија.

У Институту техничких наука САНУ је запослена од 2012. године као истраживач приправник. Ангажована је на пројекту основних истраживања ОИ172057 "Усмерена синтеза, структура и својства мултифункционалних материјала" (руководилац пројекта проф. др Владимир Павловић). 11. 10. 2013. године је изабрана у звање истраживач сарадник.

Области интересовања су јој технологија прахова, нано материјали, карактеризација материјала, полимерни материјали, математичке анализе, диелектирчна својства керамика, механичка активација, нумеричке методе.

Библиографија Адриане Пелеш

M21 међународни часопис

1. D. Kosanović, J. Živojinović, N. Obradović, V.P. Pavlović, V.B. Pavlović, A. Peleš, M.M. Ristić, "***The influence of mechanical activation on the electrical properties of $Ba_{0.77}Sr_{0.23}TiO3$ ceramics***", Ceramics International, 40, 8 Part A (2014) 11883-11888, doi:10.1016/j.ceramint.2014.04.023

2. A. Peleš, V.P. Pavlović, S. Filipović, N. Obradović, L. Mančić, J. Krstić, M. Mitrić, B. Vlahović, G. Rašić, D. Kosanović, V.B. Pavlović, ***Structural investigation of mechanically activated ZnO powder,*** Journal of Alloys and Compounds 648 (2015) 971-979, doi:10.1016/j.jallcom.2015.06.247

M22 међународни часопис

1. Z. Djurić, I. Jokić, A. Peleš, ***Fluctuations of the number of adsorbed molecules due to adsorption–desorption processes coupled with mass transfer and surface diffusion in bio/chemical MEMS sensors***. Microelectronic Engineering 124 (2014) 81–85, doi:10.1016/j.ceramint.2014.04.023

2. N. Obradović , N. Đorđević, A. Peleš, S. Filipović, M. Mitrić, V. B. Pavlović, ***The Influence of Compaction Pressure on the Density and Electrical Properties of Cordierite-based Ceramics,*** Science of Sintering, **47** (2015) 15-22, doi:10.2298/SOS1501015O

M33 Саопштење штампано у целости у изводу са међународног скупа MIEL

Z. G. Djuric, I. M. Jokic, A. Peles, "***Highly sensitive graphene-based chemical and biological sensors with selectivity achievable through low-frequency noise measurement-Theoretical considerations***", Proceedings of the International Conference on Microelectronics, *ICM* (2014

29th International Conference on Microelectronics, MIEL 2014), IEEE, 2014, pp. 153-156, http://dx.doi.org/10.1109/MIEL.2014.6842108

M34 Учешће на међународним конференцијама и семинарима

1, Jelena Živojinović, Nina Obaradović, Vera P. Pavlović, Vladimir B. Pavlović, Adriana Peleš, Momčilo M. Ristić, ***The influence of mechanical activation on the electrical properties of Ba0.77Sr0.23TiO3***, Advanced Ceramics and Application : new frontiers in multifunctional material science and processing : program and the book of abstracts : II Serbian Ceramic Society Conference, Sep 30th-Oct 1st, 2013, Belgrade (2013) (poster presentation) http://www.itn.sanu.ac.rs/opus4/frontdoor/index/index/docId/387

2. Nina Obradović, Adriana Peleš, N. Đorđević, Smilja Marković, Miodrag Mitrić, Vladimir B. Pavlović***, Influence of one activated component on the sintering process of three phase system***, The Fifteenth Annual Conference YUCOMAT 2013: Programme and the Book of Abstracts (2013), (poster presentation), http://www.itn.sanu.ac.rs/opus4/frontdoor/index/index/docId/663

3. Nataša Đorđević, A. Mihajlović, Adriana Peleš, Nina Obradović, Vladimir B. Pavlović ***Influence of MoO3 on cordierite ceramics sintering and crystallization***, The Fifteenth Annual Conference YUCOMAT 2013: Programme and the Book of Abstracts (2013), (poster presentation), http://www.itn.sanu.ac.rs/opus4/frontdoor/index/index/docId/650

4. Nebojša Labus, J. Krstić, Adriana Peleš, Jelena Živojinović, Maria Vesna Nikolić, ***Density of the ZnTiO3 nanopowder as a loose powder and as a compact obtained by different methods***, Advanced Ceramics and Application : new frontiers in multifunctional material science and processing : program and the book of abstracts : II Serbian Ceramic Society Conference, Sep 30th-Oct 1st, 2013, Belgrade (2013) (poster presentation), http://www.itn.sanu.ac.rs/opus4/frontdoor/index/index/docId/673

5. Adriana Peleš, Suzana Filipović, Vera P. Pavlović, Miodrag Mitrić, Nina Obradović, Vladimir B. Pavlović, ***The influence of mechanical activation on the structure of ZnO***, Program and the Book of Abstracts / Twelfth Young Researchers' Conference Materials

Sciences and Engineering December 11-13, 2013, Belgrade, Serbia (Oral presentation), http://www.itn.sanu.ac.rs/opus4/frontdoor/index/index/docId/695

6. Jelena Živojinović, Darko Kosanović, Nina Obradović, Adriana Peleš, Nebojša Labus, Suzana Filipović, Vladimir B. Pavlović, Miodrag Mitrić, Momčilo Ristić, ***Dilatometric Analysis of Mechanically Activated SrTiO3 Powder***, Advanced Ceramics and Application : new frontiers in multifunctional material science and processing : program and the book of abstracts : II Serbian Ceramic Society Conference, Sep 30th-Oct 1st, 2013, Belgrade (2013), (poster presentation), http://www.itn.sanu.ac.rs/opus4/frontdoor/index/index/docId/676

7. Adriana Peleš, Vera P. Pavlović, Nina Obradović, Jelena Živojinović, Miodrag Mitrić, Vladimir B. Pavlović, ***Characterization of mechanically activated ZnO powder*** , Advanced Ceramics and Application : new frontiers in multifunctional material science and processing : program and the book of abstracts : II Serbian Ceramic Society Conference, Sep 30th-Oct 1st, 2013, Belgrade, (poster presentation), http://www.itn.sanu.ac.rs/opus4/frontdoor/index/index/docId/688

8. Nina Obradović, Nataša Đorđević, Nebojša Labus, Adriana Peleš, Miodrag Mitrić, Vladimir B. Pavlović, ***Density and electrical properties of cordierite based ceramics as function of compaction pressure***, Advanced Ceramics and Application : new frontiers in multifunctional material science and processing : program and the book of abstracts : II Serbian Ceramic Society Conference, Sep 30th-Oct 1st, 2013, Belgrade (2013), (poster presentation), http://www.itn.sanu.ac.rs/opus4/frontdoor/index/index/docId/678

9. Zoran Đurić, Ivana Jokić, Adriana Peleš, ***Fluctuations of the number of adsorbed molecules due to adsorption-desorption processes coupled with mass transfer and surface diffusion in bio/chemical MEMS sensors,*** The 39th International Conference on Micro and Nano Engineering MNE 2013, 16-19 September 2013, London, UK (Poster presentation), http://www.itn.sanu.ac.rs/opus4/frontdoor/index/index/docId/820

10. Vladimir B. Pavlović, Adriana Peleš, Vera P. Pavlović, V. Đoković, R. Dojčilović, M. Dukić, B. Vlahović, ***Piezoelectric polymer/ceramic nanostructures for mechanical energy harvesting***, Advanced Ceramics and Application : new frontiers in multifunctional material science and processing : program and the book of abstracts : II Serbian Ceramic Society

Conference, Sep 30th-Oct 1st, 2013, Belgrade, (poster presentation), http://www.itn.sanu.ac.rs/opus4/frontdoor/index/index/docId/690

11. Z. Djurić, I. Jokić, A. Peleš, ***Highly Sensitive Graphene-based Chemical and Biological Sensors with Selectivity Achievable through Low-Frequency Noise Measurement-Theoretical Considerations***, 29th International conference on microelectronics, Belgrade, Serbia 12-14 May 2014 (oral presentation), http://dx.doi.org/10.1109/MIEL.2014.6842108

12. A. Peleš, S. Filipović, N. Obradović, J. Krstić, V. Pavlović, ***The morphological characterization of mechanically activated ZnO powder***, Advanced Ceramics and Aplication III, 29.09.-01.10.2014, Belgrade, Serbia (poster presentation), http://www.itn.sanu.ac.rs/opus4/frontdoor/index/index/docId/875

13. Zoran Djurić, Ivana Jokić and Adriana Peleš, ***Analyte Recognition And Quantification Based On Fluctuation Phenomena On The Active Surface Of Biochemical Sensors***, The 19th Symposium on Condensed Matter Physics - SFKM 2015, Belgrade - Serbia (poster presentation), http://www.sfkm.ac.rs/book.pdf

14. N. Tadić, A. Peleš , N. Radić , B. Stojadinović , B. Grbić , R. Vasilić , S. Stojadinović, ***Photocatalytic properties of Al_2O_3/ZnO coatings formed by plasma electrolytic oxidation on aluminum substrate,*** Advanced Ceramics and Aplication IV, 21.09.-23.09.2015 Belgrade, Serbia (poster presentation), http://www.itn.sanu.ac.rs/opus4/frontdoor/index/index/docId/1030

15. Adriana Peleš , Zoran Djurić and Ivana Jokić, ***Analysis of the low-frequency noise spectrum in graphene-based biochemical sensors and its application in analyte recognition and quantification,*** The Fourteenth Young Researchers' Conference Materials Sciences and Engineering, December 9-11, 2015. Belgrade (oral presentation), http://www.itn.sanu.ac.rs/opus4/frontdoor/index/index/docId/1022

M64 Учешће на домаћим конференцијама

1. Suzana Filipović, Nina Obradović, Vladimir B. Pavlović, Adriana Peleš, Smilja Marković, Miodrag Mitrić, Nebojša Mitrović, ***Mehanohemijska Sinteza Magnezijum Titanata***, Etran 2-5 juna 2014, Vrnjačka Banja, Srbija (poster prezentacija), http://www.itn.sanu.ac.rs/opus4/frontdoor/index/index/docId/903

Available online at www.sciencedirect.com

ScienceDirect

Ceramics International 40 (2014) 11883–11888

CERAMICS INTERNATIONAL

www.elsevier.com/locate/ceramint

The influence of mechanical activation on the electrical properties of $Ba_{0.77}Sr_{0.23}TiO_3$ ceramics

D. Kosanović[a,*], J. Živojinović[a], N. Obradović[a], V.P. Pavlović[b], V.B. Pavlović[a], A. Peleš[a], M.M. Ristić[c]

[a]Institute of Technical Sciences of the Serbian Academy of Sciences and Arts, Knez Mihailova 35/IV, 11000 Belgrade, Serbia
[b]Faculty of Mechanical Engineering, University of Belgrade, Belgrade, Serbia
[c]Serbian Academy of Sciences and Arts, Knez Mihailova 35, 11000 Belgrade, Serbia

Received 28 February 2014; received in revised form 3 April 2014; accepted 4 April 2014
Available online 15 April 2014

Abstract

Ferroelectric barium strontium titanate ($Ba_{0.77}Sr_{0.23}TiO_3$), BST, was prepared by solid-state reactions using as the starting compounds powder of barium carbonate ($BaCO_3$), strontium carbonate ($SrCO_3$) and titanium dioxide (TiO_2–anatase). Non-activated mixtures and mixtures mechanically activated in a high-energy planetary ball mill (0, 5, 10, 20, 40, 80 and 120 min) were sintered at 1100, 1200, 1300 and 1400 °C for 2 h in air atmosphere. Defects and the effect of the beginning of the sintering process on the microstructure were investigated by scanning electron microscopy (SEM). Electrical measurements (loss tangent and resistivity as the function of frequency $X_C = f(\log \nu)$) were performed for ceramics sintered at 1400 °C for 2 h. It has been found that mechanical activation can reduce the sintering temperature by around 100 °C, which leads to significant energy savings. Furthermore, activated for 80 min and sintered at 1400 °C for 2 h exhibit the largest density values and have about 36% lower dielectric loss at a frequency of 1 kHz and about 57% at a frequency of 10 kHz than the samples obtained from the initial non-activated powder sintered under the same conditions.

Keywords: A. Milling; A. Sintering; C. Electrical properties

1. Introduction

Ferroelectric ceramics are usually alkaline earth metal titanates: $BaTiO_3$, $SrTiO_3$, $CaTiO_3$, $(BaSr)TiO_3$, and Ba $(ZrTi)O_3$ [1]. Ceramic capacitors based on titanate have very high capacity and small size which enable the miniaturization of electronic devices. Among the mentioned compounds, $(BaTiO_3)_{0.65}(SrTiO_3)_{0.35}$ has the best properties, due to the large ε_r and the corresponding tgδ. The disadvantages include large and highly non-linearly changing capacitance with temperature change ($[\Delta C/C]/\Delta t$), in the operating temperature range (~55–125 °C) [2].

Barium strontium titanate, $Ba_{1-x}Sr_xTiO_3$ (BST), is a ferroelectric material with potential application in microwave devices. BST is a continuous solid solution with a tetragonal structure; it belongs to the family of (ABO_3) perovskites and it is composed of titanate, barium titanate ($BaTiO_3$) and strontium titanate ($SrTiO_3$). $BaTiO_3$ ($T_C = 393$ K) is a prototype ferroelectric which undergoes a sequence of crystal structure transitions as it switches from the ferroelectric to the paraelectric phase [3]. $SrTiO_3$ is an incipient ferroelectric i.e. it exhibits quantum ferroelectricity which means that it undergoes phase transition at very low temperatures ($T_C = 105$ K), and the quantum effect prevents complete transition to paraelectric phase [4–6].

BST is being widely investigated as a suitable dielectric material for a variety of applications including tunable RF and microwave circuits, dynamic random access memories (DRAM), bypass capacitors, and non-volatile memories [7]. Thin-film BST has several properties that make these applications possible. Most importantly, the BST films show a field-dependent permittivity.

*Corresponding author.
E-mail address: kosanovic.darko@gmail.com (D. Kosanović).

http://dx.doi.org/10.1016/j.ceramint.2014.04.023
0272-8842/

When BST is applied as a capacitor, the dielectric constant changes in a non-linear function. The nonlinearity of dielectric properties with respect to an applied dc voltage makes BST attractive for tunable microwave devices such as varistors, filters, voltage-controlled oscillators (VCO), delay lines and phase shifters [8].

The aim of this study is to investigate the influence of mechanical activation and the sintering regime on the structure and electrical properties of BST ceramics. Based on a detailed analysis of temperature dependence, loss tangent of the angle, and the influence of mechanical activation on the change of frequency characteristics, optimum technological parameters are used for obtaining $Ba_{0.77}Sr_{0.23}TiO_3$ ceramics with improved electrical characteristics.

2. Experimental procedure

Mixtures of $BaCO_3$ (99.8% p.a. Aldrich), $SrCO_3$ (99.8% p.a. Aldrich) and TiO_2 (99.99% p.a. Aldrich) powders the molar $BaCO_3$:$SrCO_3$:TiO_2=0.77:0.23:1 were mechanically activated in a high-energy ball mill (Retsch, PM 400). The process of milling was performed for 0 to 120 (0, 5, 10, 20, 40, 80 and 120) min in air atmosphere. Initial samples were milled in 500 cm^3 zirconium oxide beakers together with balls of 10 mm in diameter (the ratio of powder and balls was 1:20). After milling, the powders were dried and calcined at a temperature of 800 °C, for 4 h inside a chamber furnace.

The samples of activated and then calcined BST powders were pressed at 4 t/cm^2 (392 MPa). They were sintered in air atmosphere and in a laboratory chamber furnace (Electron) whose maximum temperature is 1600 °C. The samples were placed into the furnace and sintered at temperatures of 1100, 1200, 1300 and 1400 °C for 2 h. The heating rate was 10 °C/min, and when the furnace reached the temperatures of 1100, 1200, 1300 and 1400 °C, the pressed samples were sintered isothermally for 2 h. The morphology of sintered BST was analyzed using a scanning electron microscope (SEM, JSM-6390 LV JEOL, 25 kV).

X-ray of the sintered samples were obtained on a Philips PW 1050 diffractometer, using the λCu Kα owl radiation and the "step scan" mode with increments of 0.05°. The measurement of the dielectric loss tangent and the values of the real (R) and imaginary (X_C) components of the complex electrical impedance of the sintered samples was carried out on the device HIOKI 3532-50 LCR HiTESTER, at the operating frequency of 1 kHz and 10 kHz. The sample preparation involved the application of platinum paste on both sides of the sintered samples, which were then heated for 30 min at 150 °C with the intent of curing the paste and improving conductivity.

3. Results and discussion

The greatest changes in the density of the samples occur at 1100 and 1200 °C for samples activated for 5 min, while the effect of a prolonged milling time for 10 and 20 min is negligible at these sintering temperatures. Small changes in the density at lower sintering temperatures clearly indicate that the final stage of the sintering process occurs at higher sintering temperatures.

Table 1 shows densities of BST-S samples sintered at the following temperatures: 1100, 1200, 1300 and 1400 °C for 2 h.

Analysis of the results of isothermal sintering (Table 1) shows that the best effect is achieved by mechanical activation for 120 min at the sintering temperature of 1400 °C (Fig. 1).

The analysis of the dependence of density differences in activated and non-activated samples shows that the minimal effect of milling is observed at 1300 °C, whereas the maximum effect can be seen in the samples sintered at 1100 °C. Accordingly, energy savings are achieved using mechanical activation, which also results in good technical properties of ceramics at lower sintering temperatures.

Based on our previous results, the diffraction patterns of non-activated and mechanically activated BST isothermally sintered at 1400 °C for 2 h indicate that the phase composition of the sintered samples has four phases [9]. Well crystallized phase $Ba_{0.77}Sr_{0.23}TiO_3$ shows sharp and intense peaks and phases, such as witherite ($BaCO_3$), strontium carbonate ($SrCO_3$) and anatase (TiO_2) which occur in low concentrations. The peaks of the milled and sintered samples are reduced, which means that there is a narrowing of peaks, indicating an improved crystallinity of the samples (Fig. 2). Having in mind that the increase in the sintering temperature stabilizes the

Table 1
Sample densities, ρ_s (g/cm^3) of samples sintered isothermally at temperatures of 1100, 1200, 1300 and 1400 °C for 2 h.

Sample	1100 °C, 2 h	1200 °C, 2 h	1300 °C, 2 h	1400 °C, 2 h
BST-0	3.367	3.750	4.338	4.518
BST-5	3.643	3.939	4.393	4.606
BST-10	3.671	3.982	4.409	4.654
BST-20	3.680	3.972	4.421	4.688
BST-40	3.934	4.098	4.444	4.815
BST-80	4.118	4.199	4.526	4.941
BST-120	4.204	4.352	4.633	5.030

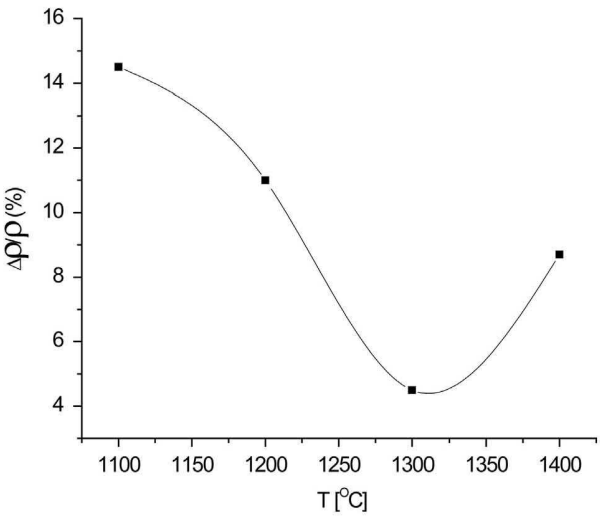

Fig. 1. Density differences in non-activated samples and the sample activated for 120 min, both sintered, as the function of the sintering temperature.

crystal structure due to the recrystallization process, it may be concluded that all of the above-mentioned facts suggest that the formation of a solid solution, the composition of which is $Ba_{0.77}Sr_{0.23}TiO_3$, has actually occurred in the system.

The analysis of the evolution of microstructural constituents during sintering, performed by scanning electron microscopy, confirms the previously presented conclusions. Based on this analysis, it has been found that an increased temperature and extended sintering time result in the related processes of grain growth and pore size reduction. Micrographs of the samples of BST-S-0, BST-S-20, BST-S-80 and BST-S-120 sintered at 1400 °C for 2 h are shown in Fig. 3.

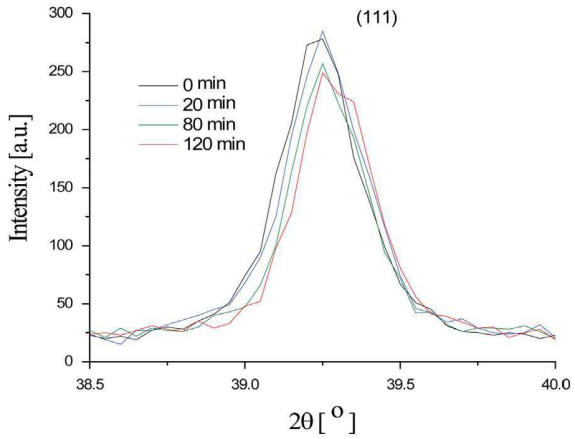

Fig. 2. Influence of the activation time on the full width at the half-maximum of diffraction lines (111) on diffractogram of sintered BST ceramics.

The SEM micrograph of the starting powder shows a large open porosity of grains of different sizes. Fig. 3a (BST-S-0) indicates the presence of larger, well-formed grains of barium strontium titanate (as one phase) and smaller grains (as the second phase). Also, in the non-activated samples, a non-homogeneous porous microstructure is observed, which is prevailed by the polygonal grain shape and the presence of the so-called texture open porosity, with pores of an irregular shape. In the sample which was mechanically activated for 20 min, uneven densification and grain growth (barium strontium titanate) have been observed (Fig. 3b). The micrograph shows the presence of a second phase (smaller particles), but they are evenly distributed. The SEM micrograph of the sample mechanically activated for 20 min shows an increased mass transport. It is caused by the higher surface activity of grain boundaries and leads to their structural reinforcement, resulting in the appearance of fracture patterns. The micrographs in Fig. 3c and d show that the increase of the activation time results in a growth of a new phase, along with the size

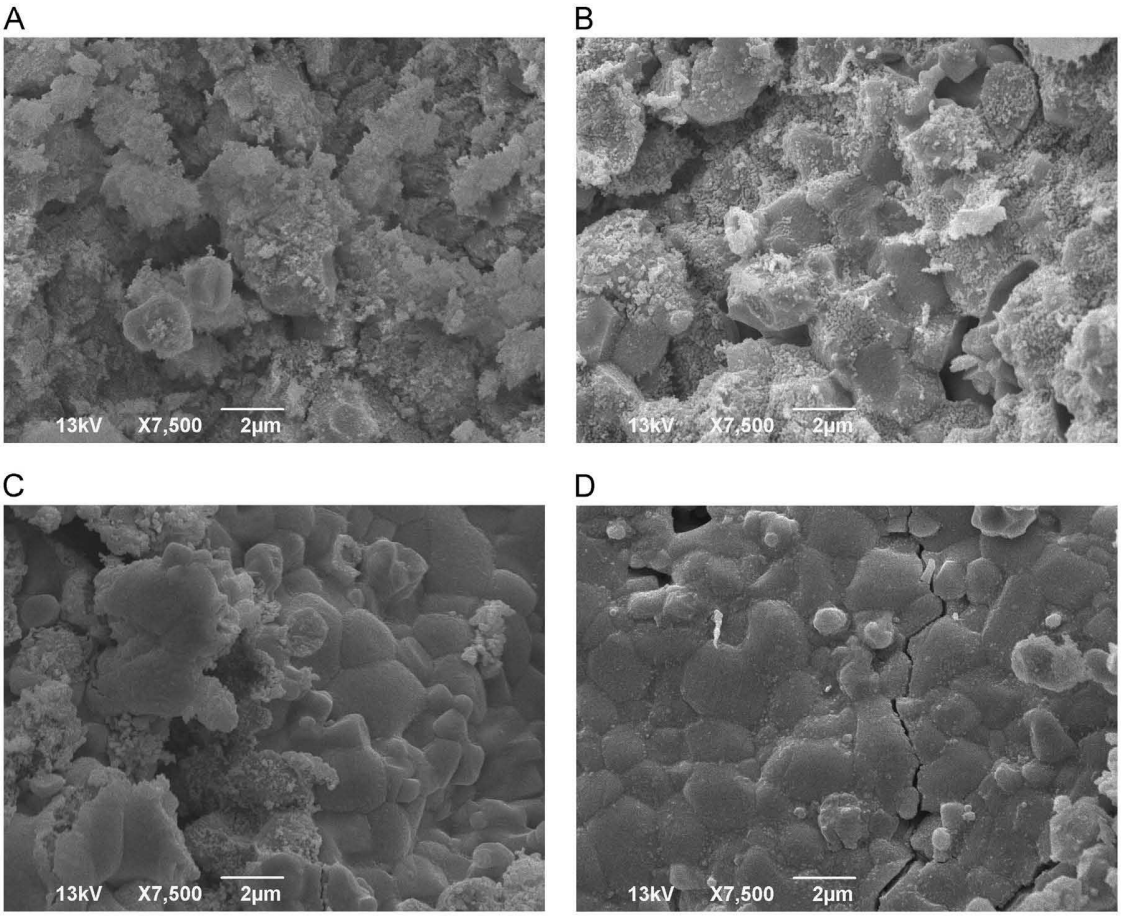

Fig. 3. Scanning electron micrographs of samples (a) BST-S-0, (b) BST-S-20, (c) BST-S-80 and (d) BST-S-120 sintered non-isothermally at 1400 °C and isothermally for 2 h.

reduction of the second phase and the reinforcement of the boundaries between grains.

Finally, the formation of the most compact structure of a polygonal shape, medium-sized with a slight presence of an unreacted second phase, has been observed. Also, there is a dominant presence of closed porosity in which spherical pores were identified, and this phenomenon shows that the system entered into the final sintering stage.

The influence of temperature on the dielectric loss in the samples $Ba_{0.77}Sr_{0.23}TiO_3$ (BST-S) sintered at 1400 °C for 2 h was considered at frequencies of 1 kHz and 10 kHz.

Based on the experimental results shown in Fig. 4, it can be concluded that tgδ increases with an increased sintering temperature (that the peaks were more pronounced). It is observed that in all sintered samples with prolonged activation times the first decline occurs in the value of the Curie-temperature, and then possibly decline in the value tgδ.

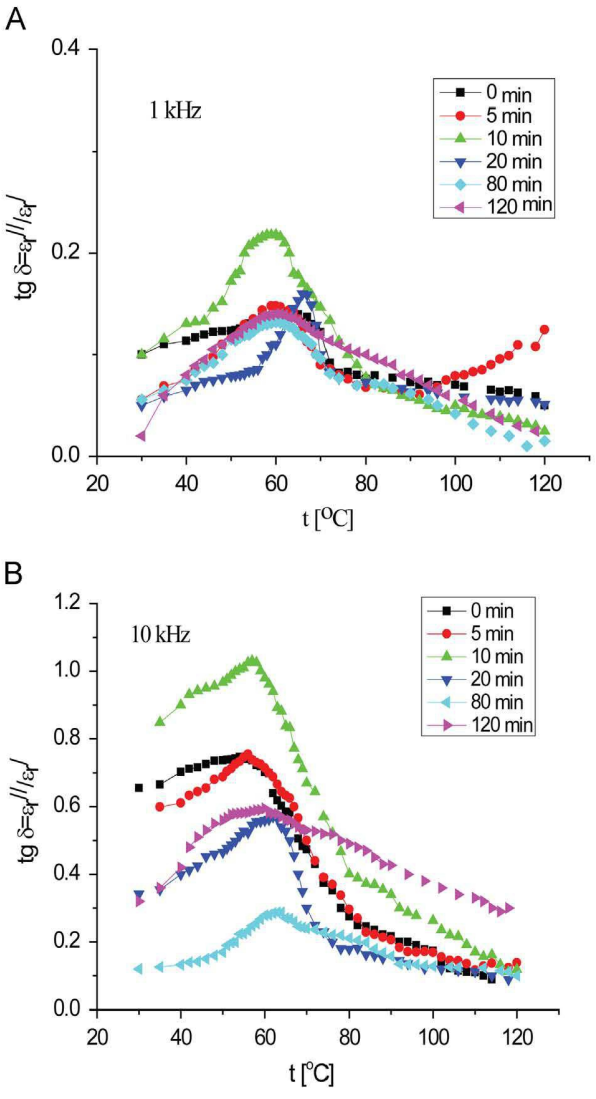

Fig. 4. Influence of the activation time on the temperature dependence of the dielectric loss in BST-S sintered samples at frequencies of (a) 1 kHz and (b) 10 kHz (system uses a dielectric loss tangent of the angle calculated from the ratio of ε_r' and ε_r'').

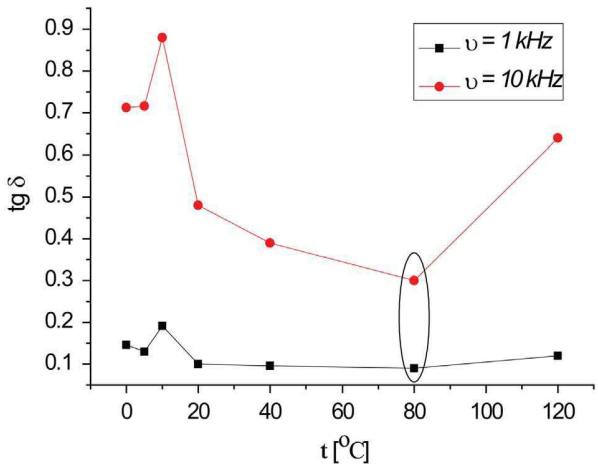

Fig. 5. Influence of the activation time on the temperature dependence of the dielectric loss in BST-S sintered samples at frequencies of 1 kHz and 10 kHz.

Based on the analysis of the results shown in Fig. 5 it can be concluded that the optimal duration of the mechanical activation of the starting powders is 80 min. The samples of the powder sintered at 1400 °C for 2 h have about 36% lower dielectric loss at the frequency of 1 kHz and about 57% at the frequency of 10 kHz than the samples obtained from the initial non-activated powder sintered under the same conditions. The dependence graphs $X_C=f(\log \nu)$ for the non-activated samples and those mechanically activated for 5, 10, 20, 80 and 120 min at temperatures from 310 to 410 °C are shown in Figs. 6–8. For the experimentally observed dependence graphs $X_C=f(\log \nu)$ for the non-activated samples and those mechanically activated for 5, 10, 20, 80 and 120 min in the paraelectrics one or two peaks appear, depending on the observed temperature and activation powders. For the temperatures of 310 and 360 °C, two peaks are observed. The first, more intense, is located in the lower frequencies and the corresponding grain boundary, and its frequency corresponds to the frequency at the top of the large semicircle in the Z^* plane. The second, less pronounced peak at higher frequencies, corresponds to the grain (Figs. 6–8).

The activated samples heated at 310 °C show a decrease in the intensity of both peaks in the frequency dependence of reactance graph $X_C=f(\log \nu)$ and the change of the position of their maxima, while the change of the intensity and position of peaks reflects the properties of the grain boundaries (Fig. 6). In the samples obtained from the powder activated for 5 min, the peak corresponding to the grain boundary decreases sharply, spreads and shifts to higher frequencies (Fig. 6a). As we move to higher frequencies, the peak corresponding to the grain also shifts, but to a considerably lesser degree; the peaks corresponding to the grain and grain boundary become closer only in terms of intensity but not in terms of position (activated samples 20, 80 and 120 min); therefore no superposition occurs.

In Fig. 7 the influence of activation time on the frequency dependence of reactance $X_C=f(\log \nu)$ at a temperature of 360 °C is shown. For the samples activated for 5 min the reduction in the intensity of both peaks, as well as the change

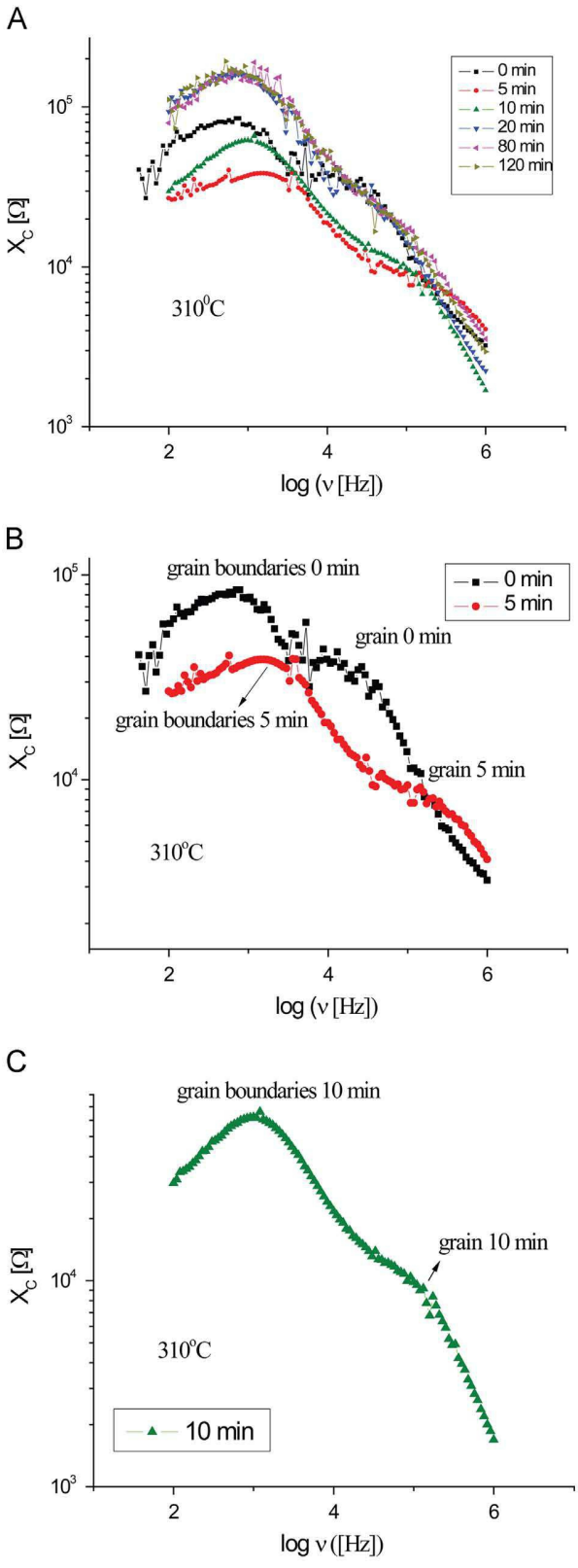

Fig. 6. Influence of activation time on the frequency dependence of reactance $X_C=f$ (log ν) at a temperature of 310 °C.

in the position of their maxima, has been compared to the non-activated sample. The samples that were activated for more than 5 min (10, 20, 80 and 120 min) show a significant

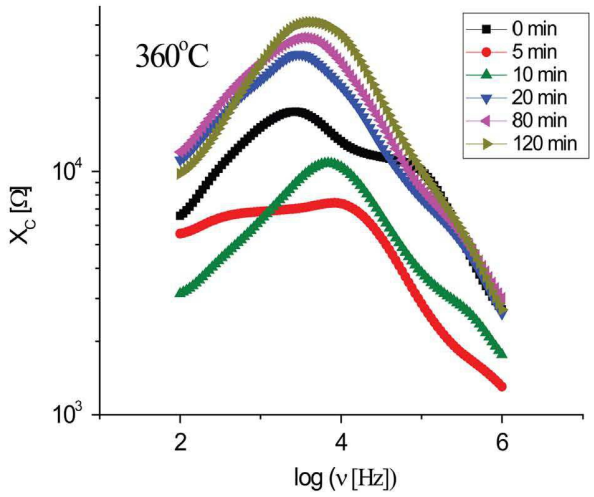

Fig. 7. Influence of activation time on the frequency dependence of reactance $X_C=f$ (log ν) at a temperature of 360 °C.

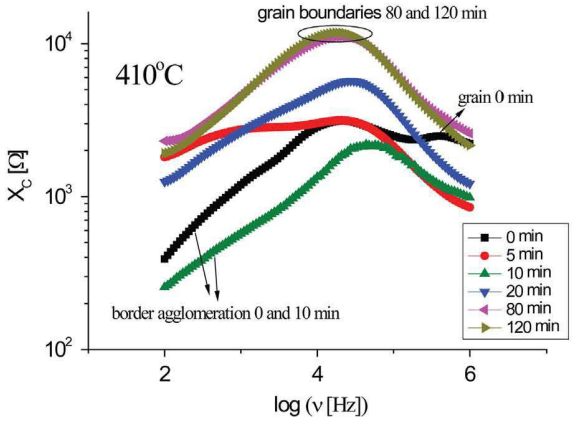

Fig. 8. Influence of activation time dependence: $X_C=f$ (log ν) at a temperature of 410 °C.

increase of the intensity peaks and their position, compared to the non-activated sample. The change of peak positions reflects the properties of grains and grain boundaries; they are shifted to lower frequencies. The changes in the peak intensities caused by activation lead to the partial overlapping of the activation patterns of the samples activated for 20, 80 and 120 min. In the samples activated for 10 min, one peak is observed, and it originates from the influence of agglomerates' boundaries.

In Fig. 8, the influence of the activation time on the frequency dependence of reactance $X_C=f$ (log ν) at a temperature of 410 °C is shown. In the samples activated for 10 min, a decrease in peak intensity and a change in the position of the maximum have been observed; at the same time mechanical activation largely brings about a change in the intensity and position of the peak which reflects the properties of grain boundaries. For the samples obtained from the powder activated for 10 min, the peak corresponding to grain boundary decreases sharply, spreads and shifts to higher frequencies (Fig. 8).

The 10-min activation results in a rapid growth and reversed directions of peak shifts, which represent the grain boundaries. This is in line with the changes in the microstructure of the samples that were previously discussed.

4. Conclusion

In this paper, the influence of mechanical activation on the electrical properties of $Ba_{0.77}Sr_{0.23}TiO_3$ ceramics has been investigated.

- Based on the measurement of the relative density of the sintered (BST-S) it has been discovered that the largest change in density occurs in the powders mechanically activated for up to 20 min and sintered at 1100 °C and 1200 °C for 2 h.
- It was found that density of BST-S samples increases with temperature and the sintering time.
- Also, the mechanical activation of the starting powder for 120 min can reduce the sintering temperature by around 100 °C, which leads to significant energy savings.
- As far as the dielectric loss is concerned, it has been found that the optimal duration of the mechanical activation of the starting powders is 80 min. The samples of the powder have about 36% lower dielectric loss at a frequency of 1 kHz and about 57% at a frequency of 10 kHz than the samples obtained from the initial non-activated powder sintering under the same conditions sintered at 1400 °C for 2 h.
- By studying the electrical properties of the BST-S sintered samples obtained from the non-activated powder heated at different temperatures (310, 360, and 410 °C) it has been found that with increasing temperatures of the sample both active and reactive components of impedance decrease.
- With the increase in temperature the relative ratio of the contribution of the grain and grain boundary resistance alters in favor of the grain boundary.

Acknowledgments

These studies were carried out within the framework of the Project OI 172057, funded by the Ministry of Education, Science and Technological Development of the Republic of Serbia and Project F/198, funded by the Serbian Academy of Sciences and Arts.

References

[1] B., Acikel, High performance barium strontium titanate varactor technology for low cost circuit applications (a dissertation submitted in partial satisfaction of the requirements for the degree of Doctor of Philosophy in Electrical and Computer Engineering), University of California, Santa Barbara, 2002.
[2] K.M. Rabe, C.H. Ahn, J.-M. Triscone (Eds.), 1st ed., Springer, Berlin, Heidelberg, 2007.
[3] E.Y. Tsymbal, Dielectric properties of insulators, PHYSICS 927: Introduction to Solid-State Physics, University of Nebraska, Lincoln, 2007 (Practice exams, lecture notes, textbooks, study guides and study materials).
[4] K. Morito, K.Y. Iwazaki, T. Suzuki, M. Fujimoto, Electric field induced piezoelectric resonance in the micrometer to millimeter waveband in a thin film $SrTiO_3$ capacitor, J. Appl. Phys. 94 (8) (2003) 5199.
[5] V. Mueller, H. Beige, H.-P. Abicht, Non-Debye dielectric dispersion of barium titanate stannate in the relaxor and diffuse phase-transition state, Appl. Phys. Lett. 84 (8) (2004) 1341.
[6] Г.А. Смоленский, В.А. Исупов, Сегнетоэлектрические свойства твердых растворов станната бария в титанате бария, Журнал технической физики 24 (1954) 1375–1386.
[7] K.M. Rabe, C.H. Ahn, J.-M. Triscone (Eds.), 1st ed., Springer, Berlin, Heidelberg, 2007.
[8] R. Thomas, V.K. Varadan, S. Komarneni, D.C. Dube, Diffuse phase transitions, electrical conduction, and low temperature dielectric properties of sol–gel derived ferroelectric barium titanate thin films, J. Appl. Phys. 90 (3) (2001) 1480.
[9] D. Kosanović, N. Obradović, J. Živojinović, A. Maričić, V.P. Pavlović, V. B. Pavlović, M.M. Ristić, The influence of mechanical activation on sintering process of $BaCO_3$–$SrCO_3$–TiO_2 system, Sci. Sinter. 44 (3) (2012) 47–55.

Journal of Alloys and Compounds 648 (2015) 971–979

Contents lists available at ScienceDirect

Journal of Alloys and Compounds

journal homepage: http://www.elsevier.com/locate/jalcom

Structural investigation of mechanically activated ZnO powder

A. Peleš [a, *], V.P. Pavlović [b], S. Filipović [a], N. Obradović [a], L. Mančić [a], J. Krstić [c], M. Mitrić [d], B. Vlahović [e], G. Rašić [e], D. Kosanović [a], V.B. Pavlović [a]

[a] Institute of Technical Sciences of SASA, Knez Mihailova 35/IV 11000 Belgrade, Serbia
[b] Faculty of Mechanical Engineering, University of Belgrade, 11000 Belgrade, Serbia
[c] Institute of Chemistry, Technology and Metallurgy, University of Belgrade, Njegoševa 12, 11000 Belgrade, Serbia
[d] Institute of Nuclear Sciences Vinca, Laboratory of Solid State Physics, 11001 Belgrade, Serbia
[e] North Carolina Central University, Durham, NC 27707, USA

ARTICLE INFO

Article history:
Received 22 January 2015
Received in revised form
20 June 2015
Accepted 27 June 2015
Available online 8 July 2015

Keywords:
Mechanical activation
N_2 physisorption
XRD
XPS
SEM
TEM
Raman spectroscopy
ZnO

ABSTRACT

Commercially available ZnO powder was mechanically activated in a planetary ball mill. In order to investigate the specific surface area, pore volume and microstructure of non-activated and mechanically activated ZnO powders the authors performed N_2 physisorption, SEM and TEM. Crystallite size and lattice microstrain were analyzed by X-ray diffraction method. XRD patterns indicate that peak intensities are getting lower and expend with activation time. The reduction in crystallite size and increasing of lattice microstrain with prolonged milling time were determined applying the Rietveld's method. The difference between non-activated and the activated powder has been also observed by X-ray photoelectron spectroscopy (XPS). XPS is used for investigating the chemical bonding of ZnO powder by analyzing the energy of photoelectrons. The lattice vibration spectra were obtained using Raman spectroscopy. In Raman spectra some changes along with atypical resonant scattering were noticed, which were caused by mechanical activation.

1. Introduction

Due to its wide direct band gap (3.37 eV) and large excitation binding energy at room temperature, ZnO is a very good semiconductor material and an important ceramic material for application in gas sensors, catalysis, solar cells and transducers [1–6]. With its wurtzite structure improved ZnO characteristics, such as smaller and more uniformed particle size, are desirable properties for its application in multilayer ceramic capacitors and varistor, as well [7]. It is well known that the structural, morphological, and electronic properties of ZnO particles depend not only on the specific crystal structure, composition, and morphology of the oxide particles, but also on defect in their structure [8]. A nanosized powder with uniformed particle size distribution and controlled particle morphology is highly desirable.

There are many methods which can produce this type of powder such as microemulsions, colloidsynthesis routes, sol–gel methods and spray pyrolysis, ion implentation, laser ablation etc. for the preparation of various nanostructures and homogenization [1]. Among these methods, to produce nanocrystalline powder and to improve the functional properties, mechanical activation has been employed, due to its simplicity, shortened time of sample preparation and low-cost.

Mechanical activation processes are used to modify the properties of materials, to enhance the reactivity of materials and to produce advanced materials etc. The reactivity of materials is dependent on different parameters such as activation time (duration time of milling process of powder) and type of energy mill. Also the different atmosphere, where the milling process is performed, has a big influence on reactivity of the material. Mechanical activation by grinding, as a method for modifying the physical and chemical properties of powder materials, is often used in powder technology [9,10]. Specific changes that occur during grinding have a great influence on final properties of the obtained material, also improving their specific application. Mechanical activation by grinding requires a few processes and mainly occurs in four stages. In the first stage there is a destruction of material than in the second stage it can be observed a formation of a new surface on the material which is destroyed. Next stage is fine grinding and finally

* Corresponding author.
E-mail address: adriana.peles@itn.sanu.ac.rs (A. Peleš).

http://dx.doi.org/10.1016/j.jallcom.2015.06.247
0925-8388/

transformation into a new material with a different structure and properties [11]. Grinding could be performed in various types of mills such as ball-mill, planetary-mill vibratory mill, pin mill etc. High-energy milling process is one of the very powerful techniques for synthesizing and particles fragmentation of all kinds of materials [12,13]. This method is widely used and it is continue to attract the serious attention of researchers.

Investigations of possible modifications of material properties are of vide interest, such as scientific and practical. A complex analysis of activated powders is necessary and requires complete information on the fine defect structure.

The goal of this research was to investigate the change in the structural characteristics of ZnO powder particles before and after milling process for shortened time (up to 30 min).

2. Experimental procedure

Commercially available ZnO powder (Sigma Aldrich, 99.9% p.a.) was mechanically activated by grinding in a high-energy planetary ball mill (Fritsch Pulverisette 7) at air atmosphere. We used wolfram carbide balls, with 5 mm in diameter, while powder to ball mass ratio was 40:1. Activation time for this study was 5, 10 and 30 min. Measurements of specific surface area and pore volume of non-activated and mechanically activated powders were carried out using Sorptomatic 1990 Thermo Electron device. Data processing was performed using the software package Advanced Data Processing Version 5.1 Release 5.13.

The microstructure morphology of all powders has been investigated using scanning electron microscopy (JEOL JSM-6390 LV) and Transmission electron microscopy (TEM, JEOL-100CX).

X-ray diffraction patterns of the initial and activated powders were obtained on a Philips PW-1050 diffractometer with λCu-K_α radiation and a step/time scan mode of 0.05°/5 s. Structural refinements were carried out using the Rietveld's method.

XPS analyses were performed using a Kratos Axis Ultra XPS system with Monochromated Aluminum K-Alpha X-Rays. The chamber vacuum during measurement was at 2.5×10^{-8} torr. The X-Ray gun was operated at 15 kW and 10 mA. A charge neutralizer was used to reduce charging effects from non-conducting surfaces. Electrons were collected at 90° from the sample surface. All survey scans were collected with a Pass Energy of 160 eV and 1 sweep (or averaging). All Region scans were performed with a Pass Energy of 20 eV. All data was calibrated to the C–C portion of the C1s peak at 284.5 eV.

Raman scattering was performed by a He–Ne laser in three different wavelengths. An 1800 lines/inch grating was used. The data was collected using a count time of 5 s with 5 averaging cycles. The samples were measured under a microscope using a 100× objective.

3. Results and discussion

It is well known that mechanical activation leads to a decrease in crystallite size, appearance of structural defects, phase transformations, order–disorder transitions, amorphisation, chemical reactions, etc. [3,13]. During the formation of mechanically activated nanocrystalline powders, in a size reduction process, powder particles brake in dependence on the applied stress and material properties [13]. The changes of the powder particle morphology and powder porosity appear during mechanical activation, manifested by interparticles void and pores within individual particles. Those changes can be analyzed by measuring pore volume and specific surface area. Our investigations showed that mechanical activation caused a significant increase in pore volume of ZnO powder. Changes in pore volume and specific surface area are shown in Fig. 1.

Applied mechanical activation introduces mechanical energy into the system, destroying the crystal structure of ZnO powder, increase the number of pores in the total porosity. Mechanical activation also changed the specific surface area. At the beginning, non-activated powder has specific surface of 6.9 m^2/g. After 5 min of activation, its value decreases to 5.9 m^2/g which is probably caused by powder particle adhesion. With prolonged milling time, values of specific surface area are increasing up to 7.8 m^2/g. These effects could be attributed to powder particle breakage, followed by increase in mesopore volume.

TEM analysis showed that the particles of non activated ZnO have polygonal shape, with smooth and uniform surfaces. As a result of mechanical activation the erosion of the surface occurred as well as diminution of the particles. It has been also noticed that for the samples activated for 30 min increased surface activity influenced the formation of agglomerates, as it can be seen in Fig. 2.

The mechanical activation led to decrease in crystallite size, increase in microstrain, introducing the energy into the system. All that changes can be observed by lowering the intensities of XRD peaks as well as its broadening. Depending on activation time these changes have been study by performing XRD, XPS and Raman analysis.

Scanning electron micrographs are in accordance with data obtained by N_2 physisorption and TEM analysis.

Fig. 3. represents SEM micrographs of non-activated ZnO powder and powders activated for 5, 10 and 30 min. Initial non-activated ZnO is a submicron powder composed of particles 0.2–0.7 microns in size with clear boundaries between the grains. A high degree of anisotropy in the shape and form of a large number of needle-shaped particles is observed. Micrograph b) and c) show that with prolonged milling time particles gained uniformed distribution, while after 30 min of activation, formation of agglomerates approximately 1 micron in size, is noticed.

The size of particles accumulated on the agglomerates surface decreases with activation time. These results are given in Table 1. At the beginning, the size covered the range between 200 and 700 nm, while with the prolonged milling time, the particle size was in the range between 60 and 470 nm.

Soft agglomerates at the surface often form in mechanically activated powders as a result of increased surface energy of mechanically activated powders. It should be notice that the formations of agglomerations during the mechanical activation can have a negative impact on sintering process to get a ceramics with good performance. The agglomeration of nanoscaled powders in general decreases the density of green bodies pressed from those

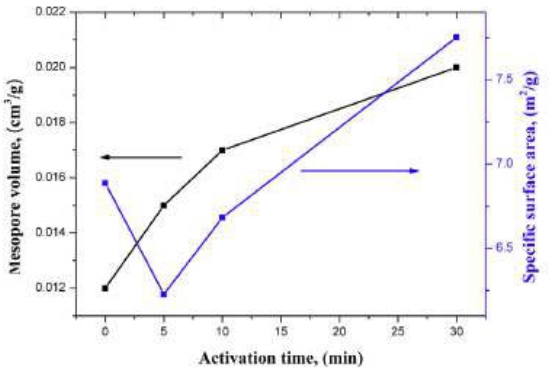

Fig. 1. Mesopore volume and specific surface area as a function of activation time.

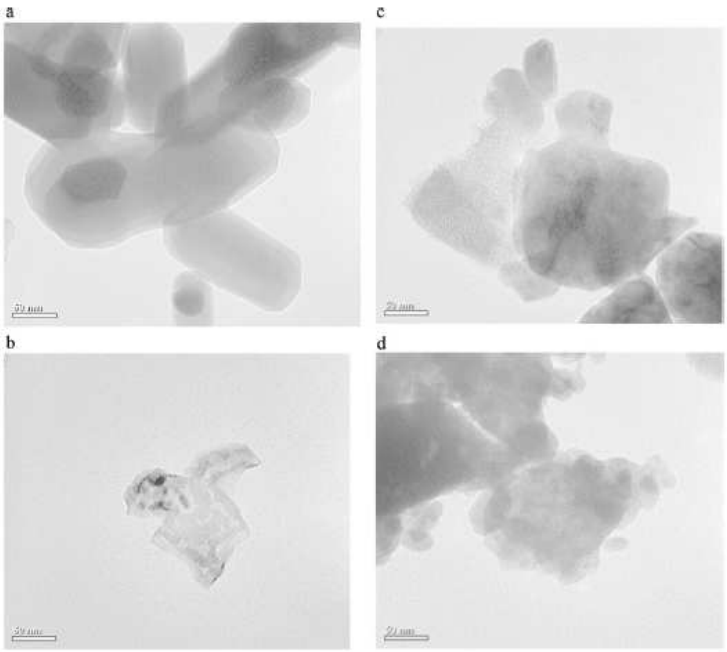

Fig. 2. TEM images of ZnO powder: a) nonactivated, b) activated for 5 min, c) activated for 10 min and d) activated for 30 min.

nanopowders. H. Ferkel and R.J. Hellmig showed in their work that a short ball-milling procedure decreases the amount of strong agglomerates in alumina and zirconia nanopowders produced with PVS and laser ablation technique [14]. In order to reduce powder agglomeration we chose the shortened time of activation, which have so far not been taken into consideration for ZnO powder.

Fig 4. represents XRD patterns of non-activated ZnO powder and the activated ones. The identification of obtained peaks has been

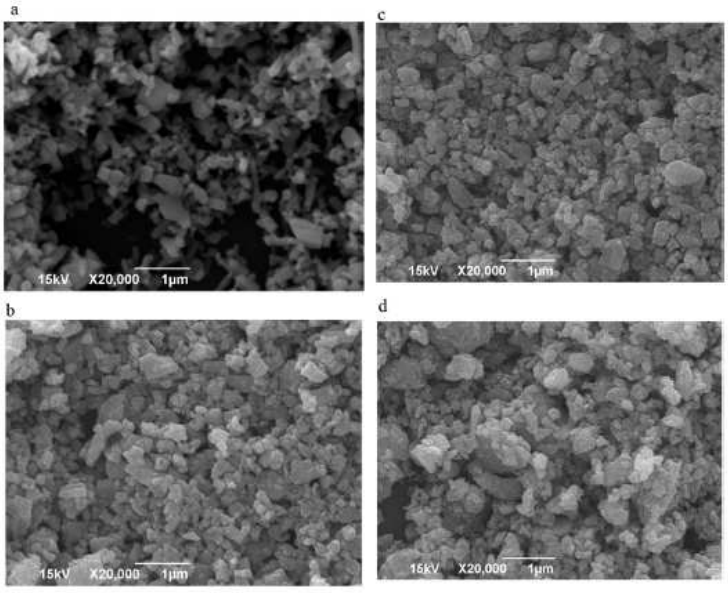

Fig. 3. SEM micrographs of ZnO powder: a) nonactivated, b) activated for 5 min,c) activated for 10 min and d) activated for 30 min.

Table 1
Particle size of ZnO powders obtained by SEM micrographs.

Activation time, (min)	Particle size, (nm)
0	212–704
5	98–545
10	76–510
30	64–464

Table 2
Lattice parameters and unite cell volume.

Activation time, (min)	a (Å)	c (Å)	v (Å^3)
0	3.25059	5.20783	47.67
5	3.25053	5.20802	47.66
10	3.25143	5.20935	47.69
30	3.25177	5.20926	47.70

performed using the ICSD card #82028 for ZnO. The tree most intensive peaks at $2\theta = 31.74°$, 34.38°, 36.22 were assigned to (100), (002) and (101) reflections of ZnO, indicating that samples were polycrystalline wurtzite structure.

Mechanical energy that introduces into the system by mechanical activation consumes an integral phase fragmentation and distortion of the crystal structure of the starting ZnO, as well as the increase of microstrain. At the beginning, large crystallites of non-activated ZnO, XRD patterns indicated sharp peaks intensities, but with prolonged milling time, those peaks intensities are getting lower along with their broadening. This may be explained by destabilization of the crystalline phase, particle refinement and crystallite size and generation of stress field [13]. This changes in peak intensity and their broadening is related to particle fragmentation and amorphization.

A process of mechanical activation is intense and energetically favorable for the producing defects within the structure. Such treatment of the powder leads to a significant increase in defects such as vacancies, dislocations, grain boundaries and they lead to change of lattice parameters and unit cell volume observed by Rietveld's method (Table 2).

X-ray powder diffraction (XRPD) patterns of the initial and activated powders were obtained on a Philips PW-1050 diffractometer with λCu-Kα radiation and a step/time scan mode of 0.05°/5 s.

Lattice parameters (a, c) and volume of the ZnO unit cell ($V = \sqrt{3}/2a^2c$) were refined from the XRPD patterns by the Rietveld method using TOPAS 4.2 software. The space group P63mc (No.186) was used as a model, with the starting values of lattice parameters and atomic positions adopted from ICSD 82028. To achieve the best fit of experimental data Fundamental Parameter Approach was applied [15]. Peak shapes, lattice parameters, and scale were refined simultaneously. After convergence, atomic positions and isotropic temperature factors were included in the refinement. Calculation of the volume weighted mean crystallize sizes, based on the individual crystallite size (D) and strain (e_{hkl}) contributions to the peak profile shapes versus 2θ (a convolution of Lorentz and Gauss functions), was done using Double-Voigt approach. Size-broadening anisotropy in whole powder pattern fitting was described by spherical harmonics. The quality of the Rietveld refinement was evaluated in terms of the discrepancy factor profile weighted residual error (Rwp < 10%) and the Goodness-of-Fit indicator (GoF ~ 1).

The influence of applied mechanical activation on crystallite size reducing and increasing of microstrain is observed. Crystallite size decreases with activation time from 60.7 nm, for non-activated powder, to 35 nm for 30 min of activation. Also, the increase of microstrain is observed, from 0.0001% for non-activated powder to 1.15% for the powder activated for 30 min. Crystallite size decreases with prolonged milling time, while lattice strain increases (Fig. 5).

XPS was used to study the electronic structure of the samples. The representative XPS spectra of O 1s and Zn 2p photoelectron lines are shown on Fig 6.

For non activated ZnO Zn2p core level spectrum comprises of a doublet Zn 2p 3/2 and Zn 2p 1/2 with symmetrical features, which rules out the presence of multi-component Zn. The doublet was fitted with two Gaussian peaks centered at 442,543 and 465,843 eV as shown in Fig. 6a, con firming the Zn^{2+} state. For the samples activated for 5 min, the main core level XPS spectrum of Zn 2p centered at ~442,186 eV and ~465,386 eV showed slightly asymmetrical features, indicating the existence of Zn in its multiple-oxidation states. The deconvoluted Zn 2p3/2 core level XPS spectrum shows two peaks, centered at ~465,432 eV and ~442,432 eV, for the samples activated for 10 min, and at ~465,375 eV and ~442,175 eV, for the samples activated for 30 min, corresponding to different oxidation states of Zn. The lower energy peak in the

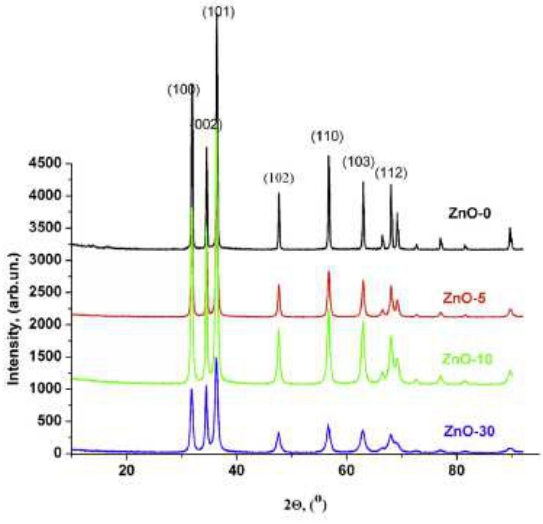

Fig. 4. XRD patterns of ZnO powders.

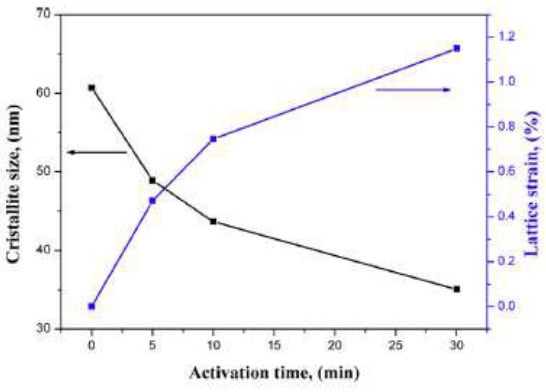

Fig. 5. Changes in crystallite size and lattice strain with activation time.

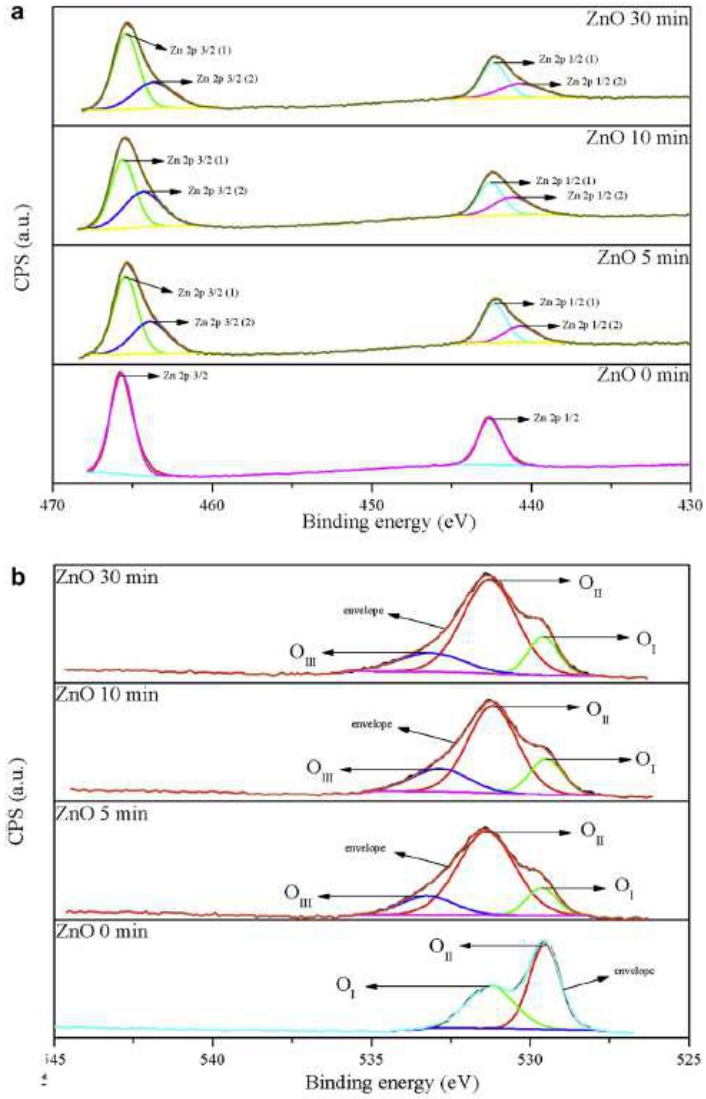

Fig. 6. XPS spectra of ZnO powders, a) Zn2p and b) O1s.

deconvoluted spectrum is attributed to the Zn^{2+} ion array surrounded by O^{2-} ions in the hexagonal ZnO and is termed as the oxide form of Zn. The deconvoluted peak centered at the higher binding energy side is related to metallic zinc. This observation is in agreement with the XPS study of ZnO:Mn nanoparticle thin films performed by U. Ilyas et al. [16], as well as with Y.Y.Chen et al. [17].

As it can be seen from the fit results of the O1s core level XPS spectra for non activated ZnO, the O 1s spectrum consists of the main peak O_I and subpeak O_{II}.The main O 1s peak O_I is attributed to O^{2-} bonded to Zn^{2+} and the subpeak O_{II} is related to OH group absorbed onto the surface of the ZnO particles. Beside those two peaks, one more peak O_{III} has been observed for the sample activated for 5, 10 and 30 min. The formation of this peak can be related to the presence of oxygen in oxygen deficient regions in ZnO host matrix, and is in accordance to the study of U. Ilyas et al. [18].

In order to study the vibrational properties of ZnO and to understand transport properties and phonon interaction with the free carriers we used Raman scattering. Also, to get the important information about the crystal structure, lattice distortion, phase transformation and defects [19]. Therefore, Raman spectroscopy techniques can be used to study the structural and morphological disorder, which are strongly correlated with optical phonons in nanostructures [20].

In the Raman spectra the non-polar E_2 (high) mode at ~438 cm^{-1} dominates, which originates from the first order scattering. This mode is primarily related to the vibrational motion of

oxygen atoms in the ZnO crystal lattice. The intensity of these modes drastically decreases with the activation time. After 30 min of activation, E_2 (high) mode expands and increases its asymmetry towards lower frequencies, indicating a disorganization of the lattice and phonon–phonon interaction [21–23].

At initial non-activated powder, there is the presence of the first order mode, a weak polar mode A_1 (TO) at ~380 cm^{-1} and the presence of a very weak polar mode A_1 (LO) at about 568 cm^{-1}. Other modes derived from multiphonons process and among them the most intensive mode is the mode of the second order ~333 cm^{-1}. Activation of the powder leads to an increase in the intensity of A_1 (LO) mode. After 5 min of activation, we begin to observe the mode at 583 cm^{-1} which we can, according to Tzolov's [24] and Wei's [25] previous investigation, ascribe to first order mode E1 (LO) and the position of the strongest mode of the second order A_1, (E_2(high) - E_2(low)) slightly shifted towards lower frequencies, from 333 cm^{-1} to 331 cm^{-1}. With the activation time an increasing in the A_1 (LO) + E_1 (LO) mode is observed. After activation of 10 min, this mode may indicate an increase in oxygen vacancies, because the increase of the concentration disrupts the long-range order in a grid, and thus leads to relaxation of Raman selection rules. Together with the peak at ~570–580 cm^{-1}, the increasing contribution of the Raman effect in the area of 545–555 cm^{-1} is observed, which is pronounced as a "shoulder" peak on the side of low frequency A_1 (LO) + E_1 (LO).

It is estimated that the activation time of 10 min or longer, this "shoulder" effect occurs as the result of two peaks. Thereby, the peak at ~545 cm^{-1}, according to literature [26–28] is associated with multiphonons process and the resulting contribution to the most convenient mode $2B_1$ low and 2LA in Γ, L, M, H point Briluenove zone. The peak at 550–560 cm^{-1} may be caused by the vibration mode so called surface optical phonons, which is theoretically confirmed by Fonoberov and Baladin [29,30], and a defect may originate from the surface of the particles as well as the effects of the boundaries between the submicron domains.

With further activation, the mutual intensity ratio of the peaks A_1 (LO) + E_1 (LO) and E_2 (high) increase, which is caused by a significant reduction in the size of the powder particles. The increase in the peak intensities of A_1 (LO) + E_1 (LO) can be caused by so-called EFI (electric field induced) Raman amplification via the "charge trapping" at the grain boundaries, combined with coupled plasma-phonon scattering. The reason of that is because the grain boundaries of polycrystalline sample come up to a certain curvature energy gap (band banding) and to the presence of a relatively strong electric field [31]. The increase in the mentioned peak can also be caused by increased presence of surface phonons. Both effects are generally more pronounced in the case of small grain size, i.e. particles of powder and crystallite [24,31], because in that case, the specific area of the observed polycrystalline sample increases. In support of the existence of the second effect is the observation that aforementioned peak $2B_1$ low mode and the existence of surface optical phonons becomes stronger and moves to 555 cm^{-1}, which may indicate an increased contribution of surface optical phonons, in relation to the activation of 10 min. This range looks like non-resonant spectrum of ZnO quantum dots ~20nm in diameter [32]. Particularly evident expansion of E_2 (high) mode and increase its asymmetry (toward lower frequencies) is arising from disorganization lattice and phonon-phonon interactions. Peak A_1 (LO) + E_1 (LO) is growing which confirms the existence of a peak $2B_1$ low. In the area of 700–2200 cm^{-1} the biggest changes occur. Modes in this range are highly amplified and the appearance of this part of the spectrum resembles the appearance of resonant amplification, although the line excitation at 633 nm (E = 1.96 eV), which is much less than the nominal band gap of ZnO (E = 3.3 eV).

In the range of 1140–1150 cm^{-1} the dominant contribution, at about 1140–1150 cm^{-1} is derived from 2E1 (LO) mode in G point Briluenove zone, which belongs to the scattering of II order. Some authors, such as Cusco and associates [33], consider that in the area of 1150–1160 cm^{-1} there is a contribution $2A_1$ (LO) mode (Overton A_1 (LO) mode) to G point Briluenove zones, and even that some contribution comes from 2LO scattering involving mixed mode the strip along the A-L-M line. In any case, there is agreement on the position that the Raman-effect of the 1140–1160 cm^{-1} does not include contributions of TO mode. Raman-effect, shows as a "shoulder" at around 1100 to 1110 cm^{-1} (Fig. 7) can be attributed to 2LO dispersed in the H and K counts Briluenove zone, while at about 1080 cm^{-1} can be note a smaller contribution of the A_1 (TO + LO). Otherwise, it is generally considered that the efficiency of Raman scattering is much higher for phonon processes involving LO mode, than processes involving TO mode. For example, Calleja and Cardona [26] reported that 2LO resonant scattering can be increased for the photon energy around ~1 eV under basic energy zone. The fact that in the mechanically activated powder practically there was no change in the intensity of A_1 (TO) mode (except for a slight weakening in the activation of the 5 min) and a significant gain of LO mode, supports the assumption of the occurrence of

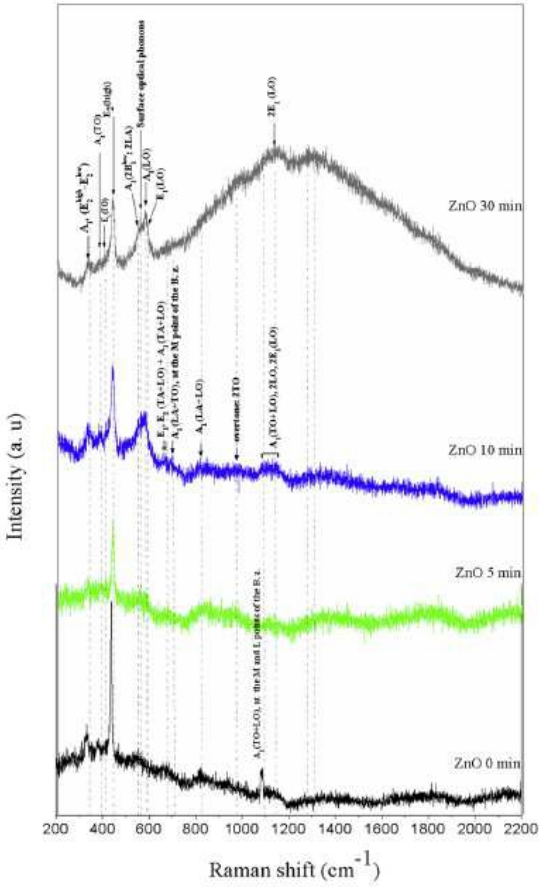

Fig. 7. Raman spectra of ZnO powders obtained with laser wavelength of 633 nm (The first and second measurement in the range above 200 cm^{-1}).

resonance amplification in the powders activated for 30 min. The Callender et al. [34], in the case of ZnO single crystals found that this mode does not depend on the wavelength of the excitation laser radiation, while the intensity E_1 (LO) mode increases significantly if there is the conditions for resonant amplification, and this coincides with what was observed in our research Powdered activated for 30 min.

This could indicate that the resonant amplification occurs through the levels in the forbidden zone [31]. Also, the appearance of the 3LO mode, i.e. the scattering of the third order in the sample ZnO – 30 min further shows the Raman resonance dispersion [31,35]. It is a resonant amplification across levels in the energy gap [23,33], which in this case is referred to the intermediate electronic states of defects created during mechanical activation.

When measuring in the range of above 20 cm^{-1} (third extended measurement) with the ZnO-activated for 30 min the phenomena E_2 (low) non-polar first order mode at 98 cm^{-1} is observed and binds the vibration zinc sublattice (Fig. 8.) [23,33]. It is observed that the modes E_2 (low) of greater intensity than the E_2 (high), which is usually the case for non-resonant scattering. To verify the above mentioned results, additional measurements were done with two more laser wavelengths, one at 442 nm and the other at 785 nm.

Figs. 9 and 10 show that the laser excitation of 785 nm appears as a typical spectrum of non-resonant scattering. In the range of 20 cm^{-1} to 800 cm^{-1} the most intense peak is E_2 (low) then E_2 (high). The influence of Raman effect at ~545–560 cm^{-1}, can be notice as a shoulder at A_1 (LO) + E_1 (LO) peak that originate from surface optical phonons. The most intensive E_2 (low) mode is related to the vibration of the zinc sublattice [21,23]. The intensity of the E_2 (low) mode is stronger than the intensity of E_2 (high) mode and this is a typical case of non-resonant scattering.

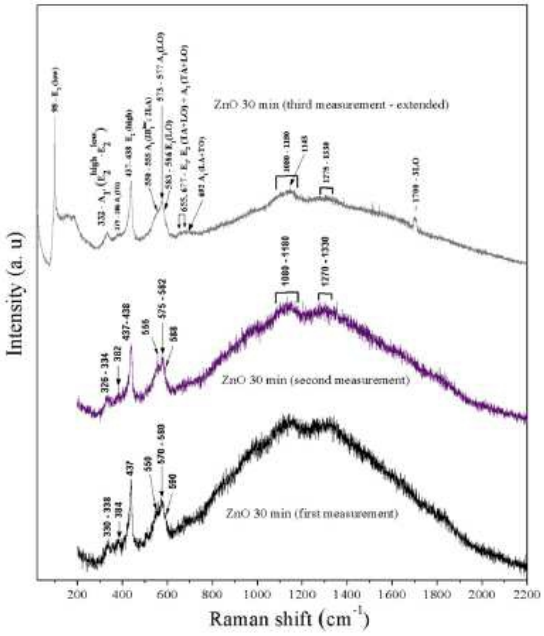

Fig. 8. Comparative graph of three different measurements of ZnO activated for 30 min.

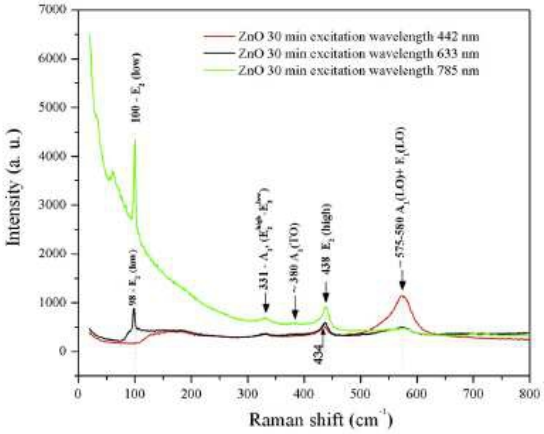

Fig. 9. Comparative graph of measurement with three different laser excitation in a range of 20–800 cm^{-1}.

Raman spectrum of the ZnO-30 sample is obtained at the laser excitation wavelength of 442 nm and looks like the resonance Raman scattering spectrum. In the range of 20 cm^{-1} to 2200 cm^{-1} (Fig. 9.) the most intense peak is A_1 (LO) + E_1 (LO) mode at 573 cm^{-1} and 578 cm^{-1}, which is due to resonant scattering, because of which and peak at ~1168 cm^{-1} derived from the mode $2E_1$ (LO) is highlighted. With activation time up to 10 min "blue shift" of peak A_1 (LO) + E_1 (LO) for more than 10 cm^{-1}, while after 30 min of activation peak goes left toward lower frequencies than non activated powder. E_2 (high) mode is getting lower whit activation time and after 30 min of activation the ratio of peaks E_2 (high) and A_1 (LO) + E_1 (LO) is equal to 1:4. E_2 (high) mode shifts to higher frequencies with activation time of 5 and 10 min. The above mentioned peak for powder activated for 30 min takes the position at a lower frequency than the non-activated powder. This is in accordance with the crystallite size (~30 nm) calculated by the Rietveld's method [22] . Blue shift of the E_2 (high) mode can be observed as extensive increase of compression type strain, concentration of defects increases which leads to the localization of phonons by defects inherent in the structure of ZnO, such as oxygen vacancies and Zn interstitial, resulting in the E_2 (high) mode and A_1 (LO) + E_1 (LO) peak shifted to the left compared to the other powders. In addition, the longest activation results in the significantly reduced size of the crystallites and changes in the dominant type of stress in terms of domination of stress-type strain, and possibly a change in the dominant type of defects, which also leads to a shift to lower-mentioned mode frequencies.

4. Conclusion

In this article the results of structural investigation of mechanically activated ZnO powders have been presented. It was noticed that mechanical activation caused the increase of mesopore volume and non-monotonic trends of specific surface area with prolonged milling time. These effects are caused by powder particle adhesion and breakage due mechanical activation. TEM images showed erosion of the surface as well as diminution of the particles and the formation of agglomerates for powder activated for 30 min. SEM micrographs are in accordance with TEM analysis, also increase of surface agglomeration to approximately 1 micron is noticed. Results obtained by Rietveld method show a significant decrease in

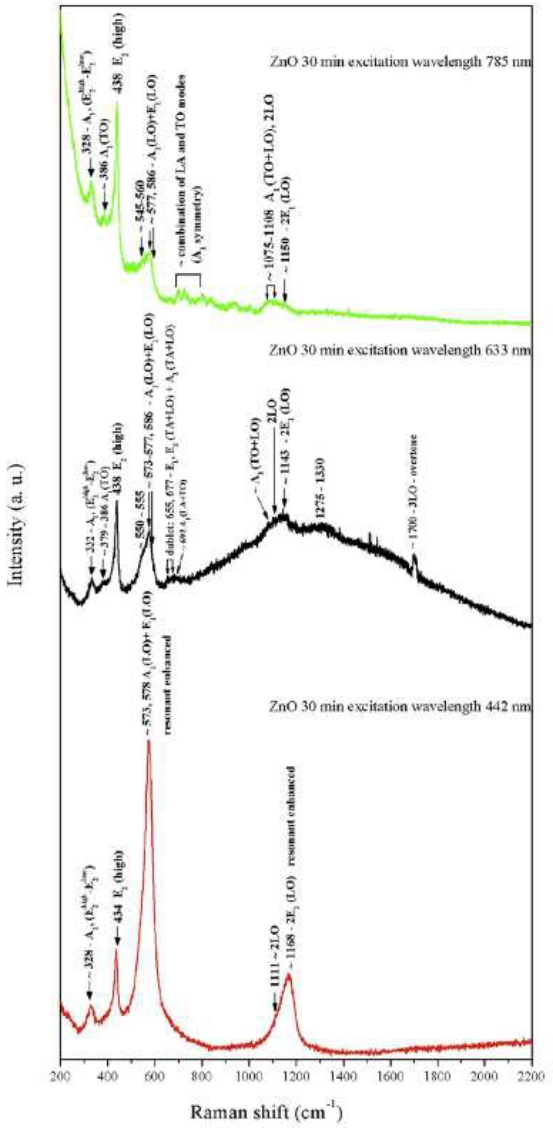

Fig. 10. Comparative graph of measurement with three different laser excitation in a range of 200–2200 cm^{-1}.

the crystallite size from ~65 to 35 nm and increase in the microstain up to 1.2%. Obtained results report the creation of defect and increase of strain inside the hexagonal lattice of ZnO powder for prolonged time of mechanical activation. For the mechanically activated samples it was noticed that the main core level XPS spectrum of Zn 2p is slightly asymmetrical. This is indicating the existence of Zn in its multiple-oxidation states. The lower energy peak in the deconvoluted spectrum is attributed to the Zn^{2+} ion array surrounded by O^{2-} ions in the hexagonal ZnO, while the deconvoluted peak centered at the higher binding energy side is related to metallic zinc. For O1s, beside two peaks (O_I and O_{II}) for non-activated powder, one more peak O_{III} has been observed for the sample activated for 5, 10 and 30 min. The formation of this peak can be related to the presence of oxygen in oxygen deficient regions in ZnO host matrix. Investigation of Raman spectra showed the "blue shift" of Raman E_2(high) mode and it lose it intensity, with activation time, as a consequence of the compression type of stress.

Unexpected "red shift" of the same Raman mode, for powder activated for the longest time, showed the intrinsic defect formation combined with confinement size effect. For the same sample it is also noticed interesting resonant Raman scattering in the range of 700–2000 cm^{-1} for initial laser wavelength of 633 nm. Obtained results indicate that mechanical activation introduced the enhancement over the levels in the gap which in our case would represent defects created during mechanical activation. In order to verify above mentioned resonant Raman scattering we applied two different laser wavelength 442 nm and 785 nm. Measurements at 442 nm confirmed "red shift" of E_2 (high) mode for powder activated for 30 min. Also it was noticed a significant shifts (10–20 cm^{-1}) of a large number of Raman mode due to activation time by laser-induced heating. The results of the non-resonant Raman scattering obtained at 785 nm are opposite of the Raman scattering at the 442 nm. This type of changes should be more investigated.

Acknowledgment

This research was performed within the projects OI 172057 financed by the Ministry of Education, Science and Technological Development of the Republic of Serbia and NSF CREST (HRD-0833184), NASA (NNX09AV07A) and Project F/198, funded by the Serbian Academy of Science and Arts.

References

[1] C.P. Fah, J. Xue, J. Wang, Nanosized zinc-oxide particles derived from mechanical activation of $Zn_5(NO_3)_2(OH)_8 \cdot 2H_2O$ in sodium chloride, J. Am. Ceram. Soc. 85 (2002) 273–275.
[2] M. Šćepanović, M. Grujić-Brojčin, K. Vojisavljević, T. Srećković, Defect induced variation in vibrational and optoelectronic properties of mamocrystaline ZnO powders, J. Appl. Phys. 109 (2011), 034313-1-8.
[3] J. Huang, Y. Wu, C. Gu, M. Zhai, Y. Sun, J. Liu, Fabrication and gas-sensing properties of hierarchically porous ZnO architectures, Sensor Actuat. B 155 (2011) 126–133.
[4] A. Stanković, Z. Stojanović, Lj. Veselinović, S.D. Škapin, S. Marković, D. Uskoković, ZnO micro and nanocrysrals with enhanced visible light absorption, Mat. Sci. Eng. B 177 (2012) 1038–1045.
[5] Z. Zang, A. Nakamura, J. Temmyo, Single cuprous oxide films synthesized by radical oxidation at low temperature for PV application, Opt. Express 21 (Issue 9) (2013) 11448–11456.
[6] Z. Zang, A. Nakamura, J. Temmyo, Nitrogen doping in cuprous oxide films synthesized by radical oxidation at low temperature, Mater. Lett. 92 (2013) 188–191.
[7] C.P. Fah, J. Wang, Effect of high-energy mechanical activation on the microstructure and electrical properties of ZnO-based varistors, Solid State Ion. 132 (2000) 107–117.
[8] V. Ischenko, S. Polarz, D. Grote, V. Stavarache, K. Fink, M. Driess, Zinc oxide nanoparticles with defect, Adv. Funct. Mater. 15 (1954) 1945–1954.
[9] N. Nikolić, T. Srećković, M.M. Ristić, The influence of mechanical activation on zinc stannate spinel formation, J. Eur. Ceram. Soc. 21 (2001) 2071–2074.
[10] M. Šćepanović, T. Srećković, K. Vojisavljević, M.M. Ristić, Modification of the structural and optical properties of commercial ZnO powder by mechanical activation, Sci. Sint. 38 (2006) 169–175.
[11] M.M. Ristić, S. Dj. Milošević, Mechanical Activation of Inorganic Materials, Serbian Academy of Sciences and Arts, Belgrade, 1998.
[12] N. Hasuike, H. Fukumura, H. Harima, K. Kisoda, H. Matsui, H. Saeki, H. Tabata, Raman scattering studies on ZnO doped with Ga andN (codoping), and magnetic impurities, J. Phys. Condens. Matter 16 (2004) S5807–S5810.
[13] V.P. Pavlović, J. Krstić, M.J. Šćepanović, J. Dojčilović, D.M. Minić, J. Blanuša, S. Stevanović, V. Mitić, V.B. Pavlović, Structural investigation of mechanically activated nanocrystalline $BaTiO_3$ powders, Ceram. Inter 37 (2011) 2513–2518.
[14] H. Ferkel, R.J. Hellmig, Effect of nanopowder deagglomeration on the densities of nanocrystalline ceramic green bodies and their sintering behaviour, NanoStructured Mater. 11 (5) (1999) 617–622.

[15] R. Cheary, A. Coelho, A fundamental parameters approach to X-ray line-profile fitting, J. Appl. Cryst. 25 (1992) 109–121.
[16] U. Ilyas, P. Lee, T.L. Tan, R.V. Ramanujan, R. Chen, H.D. Sun, R.S. Rawat, High temperature ferromagnetic ordering in c-axis oriented ZnO: Mn nanoparticle thin films by tailoring substrate temperature plasma science and applications, Int. J. Modern Phys. Conf. Ser. 32 (2014) 1460341.
[17] Y.Y. Chen, J.C. Hsu, C.Y. Lee, P.W. Wang, J. Mater. Sci. 48 (2013) 1225.
[18] U. Ilyas, R.S. Rawat, G. Roshan, T.L. Tan, P. Lee, S.V. Springham, S. Zhang, L. Fengji, R. Chen, H.D. Sun, Appl. Surf. Sci. 258 (2011) 890.
[19] Y. Huang, M. Liu, Z. Li, Y. Zeng, S. Liu, Raman spectroscopy study of ZnO-based ceramic films fabricated by novel sol-gel process, Mat. Sci. Eng. B 97 (2003) 111–116.
[20] M. Scepanovic, M. Grujic-Brojcin, K. Vojisavljevic, S. Bernik, T. Sreckovic, Raman study of structural disorder in ZnO nanopowders, J. Raman Spectrosc. 41 (2010) 914–921.
[21] K.-F. Lin, H.-M. Cheng, H.-C. Hsu, W.-F. Hsieh, Size dependence of photo-luminescence and resonant Raman scattering from ZnO quantum dots, Appl. Phys. Lett. 88 (2006), 263117-1-3.
[22] I. Calizo, K.A. Alim, V.A. Fonoberov, S. Krishnakumar, M. Shamsa, A.A. Balandin, R. Kurtz, Micro-Raman spectroscopic characterization of ZnO quantum dots, nanocrystals and nanowires, Proc. SPIE 6481 (2007), 64810N-1-8.
[23] S. Samuel, J. Koshy, A. Chandran, K.C. George, Optical phonon confinement in ZnO nanorods and nanotubes, Indian J. Pure Appl. Phys. 48 (2010) 703–708.
[24] M. Tzolov, N. Tzenov, D. Dimova-Malinovska, M. Kalitzova, C. Pizzuto, G. Vitali, G. Zollo, I. Ivanov, Vibrational properties and structure of undoped and Al-doped ZnO films deposited by RF magnetron sputtering, Thin Solid Films 379 (2000) 28–36.
[25] X.Q. Wei, B.Y. Man, M. Liu, C.S. Xue, H.Z. Zhuang, C. Yang, Blue luminescent centers and microstructural evaluation by XPS and Raman in ZnO thin films annealed in vacuum, N_2 and O_2, Phys. B 388 (2007) 145–152.
[26] J.M. Calleja, M. Cardona, Resonant Raman scattering in ZnO, Phys. Rev. B 16 (1977) 3753–3761.
[27] R. Sanz, J. Jensen, G. Gonzalez-Diaz, O. Martinez, M. Vazquez, M. Hernandez-Velez, Continuous and localized Mn implantation of ZnO, Nanoscale Res. Lett. 4 (2009) 878–887.
[28] B.H. Soni, M.P. Deshpande, S.V. Bhatt, S.H. Chaki, V. Sathe, X-ray diffraction, X-ray photoelectron spectroscopy, and Raman spectroscopy of undoped and Mn-doped ZnO nanoparticles prepared by microwave irradiation, J. Appl. Spectrosc. 79 (2013) 901–907.
[29] V.A. Fonoberov, A.A. Balandin, Interface and confined optical phonons in wurtzite nanocrystals, Phys. Rev. B 70 (2004) 233205.
[30] V.A. Fonoberov, A. Balandin, Polar optical phonons in wurtzite spheroidal quantum dots: theory and application to ZnO and ZnO/MgZnO nano-structures, J. Phys. Condens. Matter 17 (2005) 1085.
[31] Roy, S. Byrne, E. McGlynn, J.-P. Mosnier, E. de Posada, D. O'Mahony, J.G. Lunney, M. Henry, B. Ryan, A.A. Cafolla, Correlation of Raman and X-ray diffraction measurements of annealed pulsed laser deposited ZnO thin films, Thin Solid Films 436 (2003) 273–276.
[32] K.A. Alim, V.A. Fonoberov, A.A. Balandin, Appl. Phys. Lett. 86 (2005), 053103-1-3C.
[33] R. Cuscó, E.A. Uadó, J. Ibáñez, L. Artús, J. Jiménez, B. Wang, M.J. Callahan, Temperature dependence of Raman scattering in ZnO, Phys. Rev. B 75 (2007), 165202-1-11.
[34] R.H. Callender, S.S. Sussman, M. Selders, R.K. Chang, Dispersion of Raman cross section in CdS and ZnO over a wide energy range, Phys. Rev. B 7 (1973) 3788.
[35] F. Friedrich, N.H. Nickel, Resonant Raman scattering in hydrogen and nitrogen doped ZnO, Appl. Phys. Lett. 91 (2007), 111903-1-3.

Microelectronic Engineering 124 (2014) 81–85

Contents lists available at ScienceDirect

Microelectronic Engineering

journal homepage: www.elsevier.com/locate/mee

Fluctuations of the number of adsorbed molecules due to adsorption–desorption processes coupled with mass transfer and surface diffusion in bio/chemical MEMS sensors

Zoran Djurić [a,b,*], Ivana Jokić [c], Adriana Peleš [a]

[a] Institute of Technical Sciences SASA, Knez Mihailova 35, Belgrade 11000, Serbia
[b] Serbian Academy of Sciences and Arts, Knez Mihailova 35, Belgrade 11000, Serbia
[c] ICTM – University of Belgrade,Center of Microelectronic Technologies, Njegoševa 12, Belgrade 11000, Serbia

ARTICLE INFO

Article history:
Received 22 October 2013
Received in revised form 23 April 2014
Accepted 2 June 2014
Available online 10 June 2014

Keywords:
Chemical sensor
Biosensor
Adsorption–desorption
Mass transfer
Surface diffusion
Fluctuations

ABSTRACT

In this study we have developed, for the first time, the comprehensive theoretical model of the fluctuations of the number of adsorbed molecules in MEMS chemical and biological sensors, taking into account the processes of mass transfer, adsorption and desorption, and surface diffusion of adsorbed molecules. It is observed that the shape of the fluctuations spectrum contains information about various parameters of the adsorbed analyte and that even the analytes with the same affinity for the same binding sites have different spectra. The numerical calculations performed using the derived theory show that the influence of surface diffusion on the fluctuations spectrum can be significant. The practical value of this work stems from the fact that the fluctuations of the number of adsorbed molecules can be a dominant noise component in affinity-based bio/chemical sensors. Therefore, the derived theory is useful for development of the methods for the detection of analytes based on frequency domain analysis of the measured fluctuations. The recognition of an adsorbed analyte using sensors with non-functionalized sensing surface will also be considered using the presented theory.

1. Introduction

A large group of chemical and biological MEMS sensors is based on the detection of target molecules adsorbed on the active sensor surface [1]. The response of such sensors is determined by the number of adsorbed molecules, and their selectivity is achieved through functionalization of the sensing surface with specific probe molecules. The target analyte concentration and the rate constants of the interaction processes between the target and probe molecules are usually obtained from the steady state data and from the change in time of the measured parameter during the period of the steady state establishment. However, the unavoidable fluctuations of the number of adsorbed molecules also contain information about the analyte and all processes coupled with the binding reaction [2–4]. Such processes are adsorption–desorption (AD) processes, mass transfer (flow and diffusion) of the target molecules through the sensor reaction chamber to and from the surface adsorption sites [5], and surface movement (e.g. surface diffusion) of adsorbed molecules [6], as it is shown in Fig. 1a (the flow-through reaction chamber is assumed, which is the case in microfluidic devices, e.g. micro/nanofabricated sensors, such as microcantilever, as well as SPR (surface plasmon resonance), FBAR (thin Film Bulk Acoustic wave Resonator), QCM (Quartz Crystal Microbalance), graphene-based sensors etc.). The fluctuations of the number of adsorbed particles cause fluctuations of the sensor's output signal and thereby affect the sensor's ultimate performance: the total sensor noise and the minimal detectable signal. Therefore, the analysis of fluctuations is important for: 1. determination of sensor limiting performance; 2. obtaining additional information about the adsorbate and its transport and AD processes (e.g. parameters useful for adsorbed analyte recognition); 3. optimization of sensor design (the dimensions and geometry of both the sensor reaction chamber and the sensing surface) and experimental conditions (the flow rate of the sample through the reaction chamber, the surface density of the functionalization sites, etc.), with the aim of improving the sensor performance.

Experimental data show that adsorption of different types of analytes has a different influence on the spectrum of the fluctuations of the sensor signal [7,8], i.e. that the spectrum contains a

* Corresponding author at: Serbian Academy of Sciences and Arts, Knez Mihailova 35, Belgrade 11000, Serbia. Tel.: +381 11 2637367; fax: +381 11 2185263.
E-mail addresses: zdjuric@itn.sanu.ac.rs (Z. Djurić), ijokic@nanosys.ihtm.bg.ac.rs (I. Jokić), adriana.peles@itn.sanu.ac.rs (A. Peleš).

http://dx.doi.org/10.1016/j.mee.2014.06.001
0167-9317/

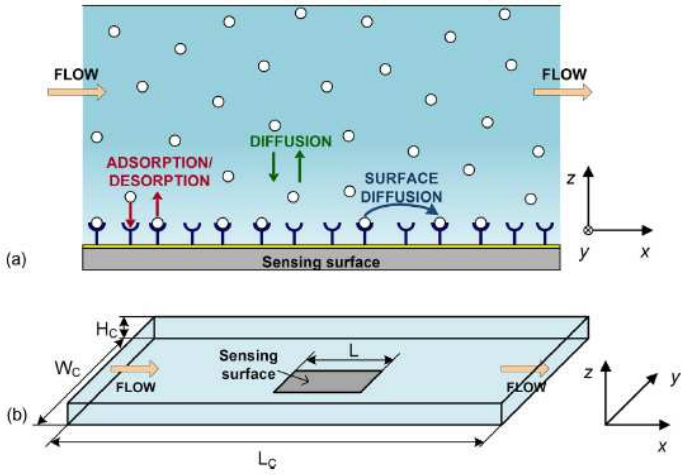

Fig. 1. Schematic representation of a bio/chemical sensor with flow-through reaction chamber: (a) the processes relevant for formation of sensor response: adsorption/desorption and transport processes of target molecules, (b) sensor system geometry.

unique adsorbate signature. This indicates that it could be possible to devise novel methods for detection of analytes based on the measured fluctuations in the frequency domain, in which it would not be necessary to functionalize the sensor surface, so the same single sensor can be used for detection and recognition of different analytes. However, a complete theoretical basis for interpretation of these experimental data does not exist. Therefore, it is impossible to be certain which of the fluctuation generation mechanisms produces the measured spectrum containing information about the adsorbed analyte. It is not known which parameters of the analyte and the processes occurring at the sensor surface, as well as the geometrical and physical parameters of a sensor determine the observed characteristic spectrum elements. Therefore, if we wish to deduce information about an analyte from the experimentally determined fluctuations spectrum and perform optimization of the sensor design, it is necessary to devise a theory of fluctuations which would take into account as many mechanisms and processes relevant for the response formation as possible.

In a recent study [2], we presented an analysis of the fluctuations of the number of adsorbed molecules taking into account the mass transfer process in biosensors in which the spatial distribution of adsorbate concentrations can be approximated by the two-compartment model. However, the measured noise spectrum suggests that noise due to surface diffusion may dominate the observed noise [9].

In this paper, we consider, for the first time, the fluctuations of the number of adsorbed molecules taking into account the processes of mass transfer, adsorption and desorption and surface diffusion of adsorbed molecules. We present the analytical expression for the spectral density of the fluctuations and the results of the quantitative analysis. Having in mind that the contribution of the fluctuations of the number of adsorbed molecules to the total sensor response fluctuations increases with decreasing dimensions of the sensor, due to which the spectrum of these fluctuations in micro and nanosensors may be dominant in certain frequency ranges, we analyze the possibility to develop new methods for analyte detection. These methods would be based on fluctuation spectrum measurements in non-functionalized sensors and use the presented theory to obtain information about the analyte from a measured spectrum.

2. Theoretical considerations

We investigate a bio/chemical sensor with a flow-through reaction chamber, in the middle of which is a sensing element, i.e. the surface of length L and area A, where binding of the target (analyte) molecules occurs (Fig. 1b). The binding site can be a functionalizing molecule immobilized on the sensing surface for the selective adsorption of the target molecule, or a non-functionalized surface adsorption site.

The binding reaction (adsorption) may occur when the analyte molecule comes in the vicinity of the surface binding site. Therefore, along with adsorption and desorption processes, analyte particle transport processes (convection and diffusion), by means of which particles are carried to and from the binding sites, are also important for the sensor response generation. While the direction of convection is determined by the sample flow through the chamber, and it is parallel to the adsorption surface, the direction of bulk diffusion depends on the spatial distribution of target analyte concentration in the chamber. The diffusion of adsorbed particles from one binding site to another (surface diffusion) occurs on the sensing surface. We introduce the following assumptions: 1. the surface density of the binding sites, n_m, is uniform; 2. only one molecule can be bound to an adsorption site; 3. all binding sites are equivalent (i.e. they have the same value of the adsorption rate constant k_f and the same value of the desorption rate constant k_r); 4. absence of any reaction between the adsorbing molecules; 5. no non-specific adsoption occurs; 6. binding coupled with transport processes leads to the formation of a thin layer depleted of adsorbing molecules adjacent to the sensing surface; 7. the steady state distribution of the adsorbed molecules is uniform on the sensing surface.

The number of the adsorbed molecules, $N(t)$, is a random process, due to stochastic nature of adsorption–desorption processes coupled with mass transfer and surface diffusion. We analyze the fluctuations ΔN of the number of adsorbed particles around the steady state value N_e. For the system geometry as shown in Fig. 1b ($L_C/W_C > 10$, $W_C/H_C > 10$), which is common in microfluidic sensing devices, it may be assumed that relevant quantities do not depend on the coordinate y [10]; accordingly, the processes of adsorption and desorption, mass transfer, and surface diffusion

at the sensing surface are linked by the following one-dimensional diffusion equation

$$\frac{\partial \Delta N}{\partial t} = \frac{\partial}{\partial x}\left(D\frac{\partial \Delta N}{\partial x}\right) - \frac{\Delta N}{\tau} \quad (1)$$

Here D is the surface diffusion coefficient, which in general can be a function of the spatial coordinates and the surface coverage. However, we assume its constant value (both in time and space), which is valid for small equilibrium surface coverages [6], small variations of the coverage around the equilibrium value, and a spatially uniform surface density of adsorbed molecules in the steady state. τ is the "lifetime" of the fluctuations of the number of adsorbed molecules

$$\tau = \left(\frac{dd_{eff}}{dN} - \frac{da_{eff}}{dN}\right)^{-1}\Bigg|_{N=N_e} = \frac{1}{k_r + k_f C} + \frac{k_r k_f n_m / k_m}{(k_r + k_f C)^2} \quad (2)$$

obtained from the effective rates of increase and decrease in the number of adsorbed molecules (a_{eff} and d_{eff}, respectively), considering AD process coupled with the mass transfer (convection and bulk diffusion) and using the two-compartment model approximation for the analyte concentration distribution in a reaction chamber (C is the concentration in the sample injected in the chamber, and k_m is the mass transfer coefficient) [2].

Using the "transport noise" approach for one-dimensional diffusion and generation-recombination processes [11,12], we have devised an analytical expression for the spectral density of the fluctuations of the number of adsorbed particles $S(f)$, $\omega = 2\pi f$, shown in the normalized form asce:display>

$$\frac{S(X)}{4<\Delta N^2>\tau} = \frac{1}{X^2}\left\{1 - \frac{1}{2\beta X}\left[(2-X)\sqrt{X+1}\left(1 - e^{-\beta\sqrt{X+1}}\cos(\beta\sqrt{X-1})\right) + (2+X)\sqrt{X-1}\,e^{-\beta\sqrt{X+1}}\sin(\beta\sqrt{X-1})\right]\right\} \quad (3)$$

where $X = (1+\omega^2\tau^2)^{1/2}$, $\beta = L/(2D\tau)^{1/2}$, $<\Delta N^2> = k_r k_f C n_m A\tau/(k_r + k_f C)$.

The obtained expression shows the influence of various parameters on the spectral density, thus enabling us to investigate both the separate influences of AD, mass transfer and surface diffusion, and their combined effect on the fluctuations spectrum.

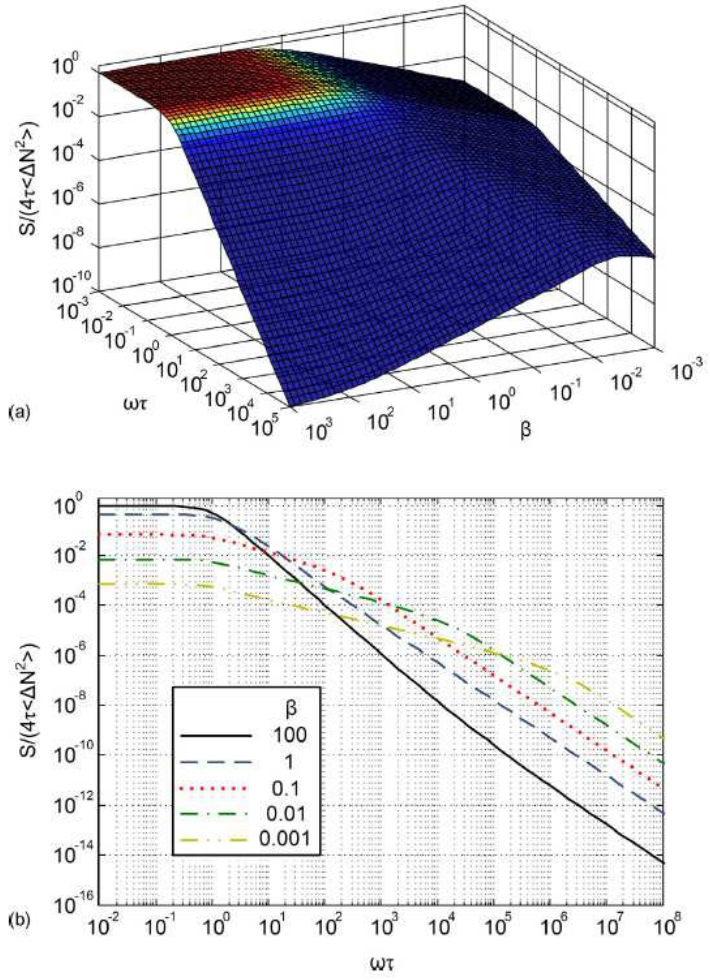

Fig. 2. Normalized spectral density of the fluctuations of the number of adsorbed molecules as the function of the parameters $\beta = L/(2D\tau)^{1/2}$ and $\omega\tau$: (a) 3D diagram, (b) the cross-sections of the 3D diagram for five different values of β.

Starting from Eq. (3), known expressions valid for two limiting cases can be obtained:

1. when the diffusion time constant $\tau_D = L^2/(2D)$ is much greater than τ, Eq. (3) is transformed into the expression for the fluctuations spectral density for the case of AD process coupled with mass transfer [2]

$$S_{AD,MT}(f) = \frac{4 < \Delta N^2 > \tau}{1 + (2\pi f)^2 \tau^2}$$

2. when $\tau_D \ll \tau$, Eq. (3) is transformed into the expression for the spectral density of fluctuations due to surface diffusion [11,3]

$$S_{SD}(\theta) = \frac{N_e L^2}{D\theta^3}\left[1 - e^{-\theta}(\cos\theta + \sin\theta)\right]$$

where $\theta = L(\omega/(2D))^{1/2}$.

3. Results of numerical calculations and discussion

Using the presented theoretical model, an analysis is performed in order to estimate the influence of the surface diffusion on the spectrum of the fluctuations of the number of adsorbed molecules.

Figs. 2a and b show the normalized spectral density of the fluctuations of the number of adsorbed molecules as the function of the parameters $\beta = L/(2D\tau)^{1/2} = (\tau_D/\tau)^{1/2}$ and $\omega\tau$. A change in the shape of the fluctuations spectrum depending on the ratio of the constants τ_D and τ can be observed. While the first frequency ($\omega_{c1} = 1/\tau$) at which the decrease in the magnitude of the spectral curve is observed in the presented diagrams is determined by the time constant τ (which means that it does not depend on surface diffusion), different values of surface diffusion parameters influence the low-frequency ($\omega \ll 1/\tau$) value of the fluctuations spectrum and the shape of the curve at frequencies $\omega > 1/\tau$. It can be concluded that the influence of surface diffusion on the fluctuations spectrum becomes significant for $\beta < 0.1$. Then another frequency, ω_{c2}, is observed at which the spectral curve bends, and its value is determined by the constant τ_D. In the presented diagrams it can be seen that $\omega_{c2} > \omega_{c1}$. In particular, for a given analyte (i.e. for a constant diffusion length $(D\tau)^{1/2}$) the influence becomes more prominent if the characteristic dimension (length L) of the sensing surface is smaller.

Fig. 3 shows the normalized spectral density of the fluctuations multiplied by f, for three different analytes and one single sensor of the characteristic length $L = 2$ μm. The parameters of the adsorbates are $\tau_1 = \tau_2 = \tau_3 = 100$ s, $D_1 = 6.5{\cdot}10^{-9}$ m^2/s, $D_2 = 1.8{\cdot}10^{-9}$ m^2/s, $D_3 = 3.5{\cdot}10^{-11}$ m^2/s. The values are selected with the idea of applying the presented theory on actual analytes and in an actual device. We used the experimental results shown in Ref. [8], obtained by measuring the spectrum of fluctuations of the output signal of the graphene chemical sensor in the presence of different analytes. The experimental value for the time constant τ is of the order of 100 s [8]. Since it has been experimentally demonstrated that the maximum of the spectrum multiplied by f indicates the type of the analyte, we use the expression derived for the fluctuations spectrum in order to obtain the frequency f_{max} where the maximum of the function $f{\cdot}S$ occurs. The derived approximate expression is $f_{max} \approx 0.59D/L^2$. By using this expression and the values of f_{max} experimentally obtained in [8] for acetonitrile, methanol and tetrahydrofuran, we obtained the above values for the analyte diffusion coefficients D_1, D_2 and D_3, respectively. The corresponding diffusion time constants equal $\tau_{D1} = 3{\cdot}10^{-4}$ s, $\tau_{D2} = 10^{-3}$ s, and $\tau_{D3} = 0.057$ s; accordingly, $\tau_D \ll \tau$, and the fluctuations spectrum is predominantly determined by the surface diffusion. The inset in Fig. 3 shows for the same three analytes the calculated spectral density of the sensor noise, S_{TOT}, multiplied by f, which takes into account $1/f$ noise together with the noise due to fluctuating number of adsorbed particles. The latter is obtained by applying the theory presented in this paper, while the parameters of the $1/f$ noise spectral density used in the calculations are determined using the experimentally obtained curves for a graphene-based gas sensor [8]. The curves shown in the inset are in good agreement with the experimentally obtained curves shown in [8]. This agreement between theoretical and experimental results could mean that the maximum obtained experimentally originates from

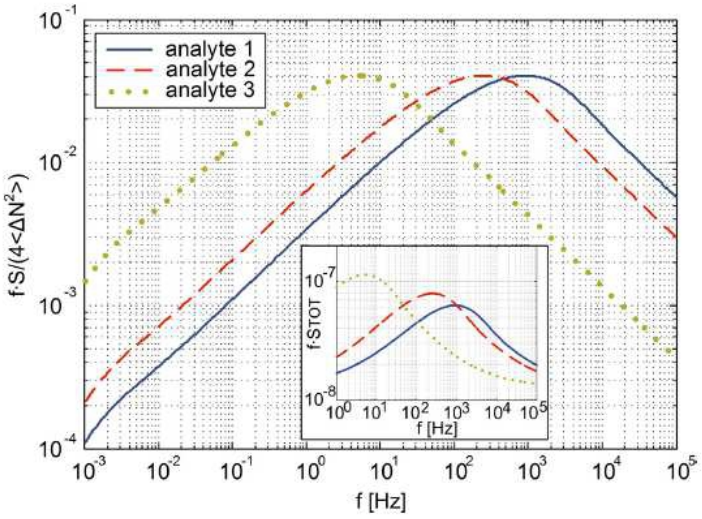

Fig. 3. The normalized spectral density of the fluctuations multiplied by f, for three different analytes, with the parameters $D_1\tau_1 > D_2\tau_2 > D_3\tau_3$. The inset shows the calculated spectral density of the sensor noise for the same three analytes, S_{TOT}, multiplied by f, which takes into account $1/f$ noise together with the noise due to fluctuating number of adsorbed particles.

the fluctuations in the number of adsorbed particles, caused by surface diffusion, the AD process and bulk mass transfer.

It is observed in Fig. 3 that the frequency which corresponds to the maximum of the function $f \cdot S$ differs for different analytes. Hence the fluctuations spectrum contains information about the analyte that can be used in its identification. It can be concluded from the example given in Fig. 3 that it is possible to distinguish between different analytes, including those that have a similar affinity for binding to the same adsorption sites (the same τ for the three analytes in the example), based on the frequency of the maximum, if they have different surface diffusion constants. This opens possibilities for the development of novel methods for detection of various analytes using a single non-functionalized sensor, based on the fluctuations spectrum measurement.

4. Conclusion

A theoretical model of the fluctuations of the number of adsorbed molecules in MEMS bio/chemical sensors is devised, taking into account the processes of adsorption and desorption, mass transfer, and surface diffusion of target molecules. The performed numerical analysis provides an insight into the qualitative and quantitative influence of surface diffusion on the spectrum of the fluctuations. It is shown that this influence increases for smaller diffusion time constants. For a given analyte the influence of surface diffusion becomes more prominent if the characteristic dimension (length) of the sensing surface is smaller. It is also observed that the shape of the fluctuations spectrum contains information about various parameters of the adsorbed analyte and that even the analytes with the same affinity for the same binding sites have different spectra.

The practical value of this study stems from the fact that the fluctuations of the number of adsorbed molecules in micro/nanosensors can dominate over other fluctuation generating mechanisms in a certain frequency range. Therefore, the derived theory is useful for development of methods for detection and characterization of analytes based on frequency domain analysis of the measured fluctuations. Especially interesting is the applicability of this theory for analyte recognition based on the fluctuations spectrum, which enables detection of multiple analytes using a single non-functionalized sensor. Furthermore, the presented theory may be used for estimation of the sensor's limiting performance.

Acknowledgments

This work was partially funded by the Serbian Academy of Sciences and Arts (Project F/150) and the Serbian Ministry of Education, Science and Technological Development (Projects TR 32008, OI172057).

References

[1] T.R.J. Holford, F. Davis, S.P.J. Higson, Biosens. Bioelecton. 34 (2012) 12–24.
[2] I. Jokić, Z. Djurić, M. Frantlović, K. Radulović, P. Krstajić, Z. Jokić, Sens. Actuators B 166–167 (2012) 535–543.
[3] G. Schmera, L.B. Kish, Sens. Actuators B 93 (2003) 159–163.
[4] E. Lutgens, A. Janshoff, ChemPhysChem 6 (2005) 444–448.
[5] T.M. Squires, R.J. Messinger, S.R. Manalis, Nat. Biotechnol. 26 (2008) 417–426.
[6] T. Ala-Nissila, R. Ferrando, S.C. Ying, Adv. Phys. 51 (2002) 949–1078.
[7] G. Zheng, X.P.A. Gao, C.M. Lieber, Nano Lett. 10 (2010) 3179–3183.
[8] S. Rumyantsev, G. Liu, M.S. Shur, R.A. Potyrailo, A.A. Balandin, Nano Lett. 12 (2012) 2294–2298.
[9] Y.T. Yang, C.C. Callegari, X.L. Feng, Y.L. Roukes, Nano Lett. 11 (2011) 1753–1759.
[10] R. Hansen, H. Bruus, T.H. Callisen, O. Hassager, Langmuir 28 (2012) 7557–7563.
[11] C.M. van Vliet, J.R. Fasset, Fluctuations due to electronic transitions and transport in solids, in: R.E. Burgess (Ed.), Fluctuation Phenomena in Solids, Academic Press, New York, 1965, pp. 267–352.
[12] C.M. van Vliet, IEEE Trans. Electr. Dev. 41 (1994) 1902–1915.

Science of Sintering, **47** (2015) 15-22

doi: 10.2298/SOS1501015O

UDK 549.632; 622.785

The Influence of Compaction Pressure on the Density and Electrical Properties of Cordierite-based Ceramics

N. Obradović[1,*)] , N. Đorđević[2], A. Peleš[1], S. Filipović[1], M. Mitrić[3], V. B. Pavlović[1]

[1]Institute of Technical Sciences of SASA, Knez Mihajlova 35/IV, 11000 Belgrade, Serbia

[2]Institute for Technology of Nuclear and Other Mineral Raw Materials, Bulevar Franse d'Eperea 86, 11000 Belgrade, Serbia

[3]Vinča Institute of Nuclear Sciences, University of Belgrade, Mike Alasa 12-14, 11000 Belgrade, Serbia

Abstract:

Due to its characteristics, cordierite, $2MgO{\cdot}2Al_2O_3{\cdot}5SiO_2$, is a high-temperature ceramic material of a great scientific interest. Mechanical activation of the starting mixtures containing 5.00 mass% TiO_2 was performed in a high-energy ball mill for 10 minutes. The compaction pressure varied from 0.5 to 6tcm^{-2} (49–588 MPa). The sintering process was performed at 1350°C for four hours in the air atmosphere. The phase composition of the activated and sintered samples was analyzed using X-ray diffraction. Scanning electron microscopy was used to analyze the microstructure of both compacted and sintered samples. The authors have investigated the influence of compaction pressure on the sintered samples and their electrical properties.

Keywords: *Mechanical activation, Density, XRD, SEM, Electrical properties, Cordierite.*

1. Introduction

Cordierite-based ceramics, with the basic chemical composition of $2MgO{\cdot}2Al_2O_3{\cdot}5SiO_2$, are widely used in various fields, from substrates for micro-electronic packaging industry to cookware, heat exchangers, glazes for floor tiles, etc. Owing to its low-temperature thermal expansion coeficient ($20{\cdot}10^{-7}°C^{-1}$) and low relative dielectric constant (~5), these ceramic materials are also well-known by their good thermo-mechanical, chemical and dielectric properties [1,2]. Therefore, these could be applicable as materials exposed to sudden temperature changes [3-7] and also as semiconducting bearers [8,9].

Our previous studies [10] show that the mechanical activation of starting components (kaolin, quarz, magnesium oxide) has a significant impact on the lowering of the sintering temperature. It has been demonstrated that, compared to non-activated components, mechanically activated ones increase energy due to induced crystal defects. During a mechanochemical treatment, several processes occur: attrition of the starting material, crystal lattice destruction, the formation of various defects, etc. All of the mentioned proccesess increase the chance for reactions to occur at temperatures lower than usual [11]. Furthermore, mechanical activation could affect the final electrical characteristics; accordingly, it is very

*) **Corresponding author**: obradovic.nina@yahoo.com

important to take into account and understand the changes that are introduced into the system during milling.

The application of compaction pressure is an unavoidable technological procedure in the sintering process [12-15]. The importance of this procedure is obvious, having in mind that pressure conditions have an influence on intergranular contacts, which play an important role in the sintering process. The initial density of samples is one of the essential parameters and it has an important role in the final characterization of the microstructure. Along with the applied pressure, the packing of powder particles is also the function of the material's class, the shape of primary particles and the strenght of interparticle connections, etc. [13,16].

In this paper, the authors have investigated the influence of compaction pressure on the density and the microstructure of mechanically activated powders as well as the density and electrical properies of the sintered samples.

2. Experimental procedure

In these experiments, authors used $Mg(OH)_2$, Al_2O_3, SiO_2 and TiO_2 (all p.a. purity). The mixture of $MgO+Al_2O_3+SiO_2$ in the 2:2:5 ratio, with the addition of 5.00 mass% TiO_2, was mechanically activated by grinding in a high-energy planetary ball mill. ZrO_2 vessels and balls with the powder-to-balls mass ratio of 1:40 were used. The milling process was performed in the air atmosphere for 10 minutes. The samples were denoted as K-10, according to the milling time. The X-ray powder diffraction patterns after milling and sintering were obtained using a Philips PW-1050 diffractometer with $\lambda Cu\text{-}K_\alpha$ radiation and a step/time scan mode of 0.05^o $1s^{-1}$. The morphology of the obtained powders and sintered samples was characterized by scanning electron microscopy (JEOL JSM-6390 LV). The powders were crushed and covered with gold in order to perform these measurements.

The pressure used in our experiments was 0.5–6 tcm^{-2} (49–588 MPa). The amount of the samples was 0.30 g. The pressure was performed in a double-sided tool 6 mm in diameter (Hydraulic press RING 14, VEB THURINGER). The density of the specimens was calculated from the measurements of their diameter, thickness, and mass. The theoretical density (TD) of the mixture was 3.078 gcm^{-3} and was calculated based using the following equation:

$$\rho_{mixture} = \frac{m_{mixture}}{V_1 + V_2 + V_3 + V_4} \quad (1)$$

where: m is the mass of the mixture (30.00 g), V_1, V_2, V_3 and V_4 are the volumes of Component 1 – MgO, Component 2 – SiO_2, Component 3 – Al_2O_3 and Component 4 – TiO_2 in the mixture, respectively, calculated using the TD of the components.

The compacts were placed in an alumina boat and heated in a tube furnace (Lenton Thermal Design Typ 1600), and then sintered isothermally at 1350ºC in air atmosphere for four hours; the heating rate was $10ºCmin^{-1}$.

The electrical properties of the sintered samples were measured on 4262A LCR meter Hewlett Packard aparatus, at the frequency of 10 kHz.

3. Results and discussion

The results obtained after compaction are presented at Tab. I and Fig. 1. The density values were increased with the applied pressure and the greatest density was obtained after the compaction process at $6tcm^{-2}$.

Tab. I Density of green bodies obtained during the compaction of the cordierite powder with the addition of TiO_2 activated for 10 minutes.

P (tcm^{-2})	ρ (gcm^{-3})	TD (%)	ρ_{rel} (%)	Π
0.5	1.8647	60.58	0.6058	0.3942
1	1.9110	62.09	0.6209	0.3791
2	2.0090	65.27	0.6527	0.3473
3	2.0540	66.73	0.6673	0.3327
4	2.0885	67.85	0.6785	0.3215
5	2.1227	68.96	0.6896	0.3104
6	2.1500	69.85	0.6985	0.3015

P – compaction pressure, ρ – green-body densities, TD – sample density as percentage of the theoretical density, ρ_{rel} – relative density, Π – sample porosity, $(1-\rho_{rel})$

The R. Panelli and F. Ambrozio Filho [17] equation is used in order to fit the obtained density values:

$$\ln\left(\frac{1}{1-D}\right) = AP^{\frac{1}{2}} + B \qquad (2)$$

where: P is compaction pressure, D is the relative density, A is the parameter showing the powder's abillity for compaction by plastic deformation and B is the parameter related to the density before compaction. The values of parameters A and B, obtained by fitting the experimental data using the Table Curve programme package are: A - 0.1785 and B - 0.7888.

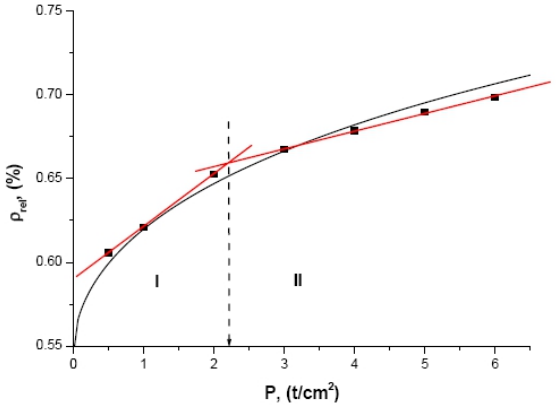

Fig. 1. Relative density values as a function of pressure fitted (black curve) by the Panelli-Ambrozio Filho equation [17].

The authors of the compaction equation [17] state that parameter A (the slope of the curve) determines the plastic deformation ability of a powder. The higher the A parameter, the greater is deformation within the powder. Parameter B is a y-axis intercept, or the density of the powder with no pressure applied. Plastic materials have higher values of A, while brittle materials have lower A values. If we compare the results obtained in our previous studies [18] for other materials, such as oxides of Zn, Ti, Mg, we may conclude that this powder shows plastic deformation. However, if we take into account the complexity of this four-component system, the inability of the equation to fit complex systems and the fact that fitting results are not satisfactory, we can divide our results in two categories (two lines in Fig. 1). The first (I) covers the first phase of three pressures (0.5, 1 and $2tcm^{-2}$), while the second (II) extends over

the second phase (3 – 6tcm^{-2}). The intersection of these two straight lines should clearly represent the distinction of two mechanisms to whose agency the powders are exposed during the compaction process. The first one is assigned to rearranging due to particles' mutual rapprochement and the second is the deformation breaking of powder particles [19].

The diffraction pattern for the K-10 mixture showed the presence of the starting components ($Mg(OH)_2$, SiO_2, Al_2O_3, AlO(OH) and TiO_2) [10]. Most peak intensities decreased during a 10-minute activation process, while some peaks were broadened, which indicated that processes of crystal lattice destruction, along with the amorphization, have started. This is in accordance with the results obtained after the calculations of microstructure parameters based on the approximation method. The crystallite size, calculated using Scherrer's equation, decreased from 63 to 48 nm for alumina, from 76 to 57 nm for silica, from 55 to 47 nm for titanium and from 53 to 46 nm for magnesium, during a 10-minute activation process.

Fig. 2. shows the SEM micrographs of the cordierite powder activated for 10 minutes and pressed under a) 0.5, b) 3 and c) 6 t/cm^2.

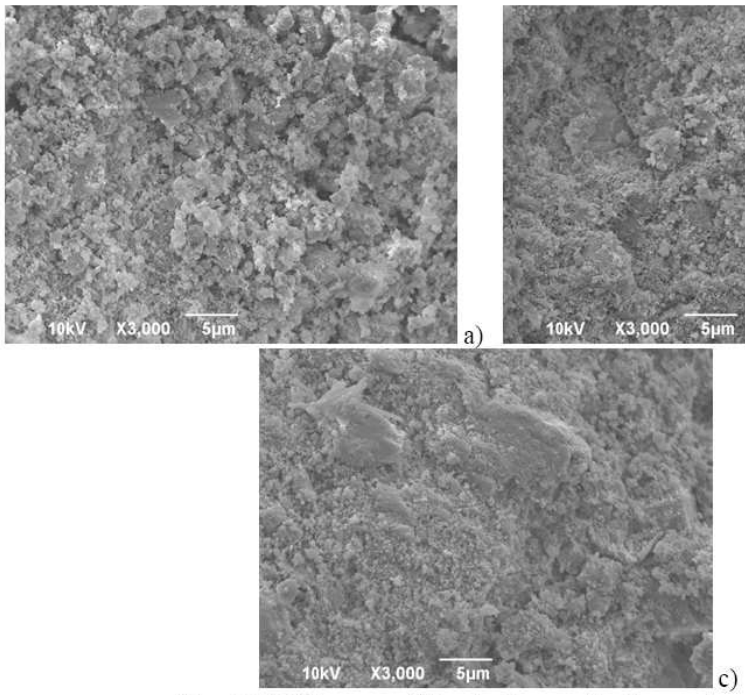

Fig. 2. SEM images of the starting cordierite powder pressed under a) 0.5, b) 3 and c) 6t/cm^2.

The powder pressed under 0.5tcm^{-2} shows considerably high porosity and great voids between particles are noticeable. Powder particles are clearly defined and the surface on compact breaks is rough. With the increased pressure, powder particles are getting closer and defined agglomerates can be observed. It is clearly visible that samples pressed under 6tcm^{-2} have a denser structure and an increased number of mutual contacts. The porosity also decreases and the shape of single particles is not so visible; it is right to say that blocks of agglomerates are formed, due to higher pressures.

Fig. 3. shows the SEM micrographs of the compacts pressed under a) 0.5, b) 3 and c) 6 tcm^{-2} pressure, sintered at 1350°C for four hours. According to the presented SEM micrographs, we have obtained the expected results regarding the microstructure of the

sintered samples. Fig. 3. a) shows a small-grain structure with an open porosity. The sintered samples pressed under the pressure higher than 2tcm^{-2} show the greatest change in microstructures, which is in accordance with Fig. 1.

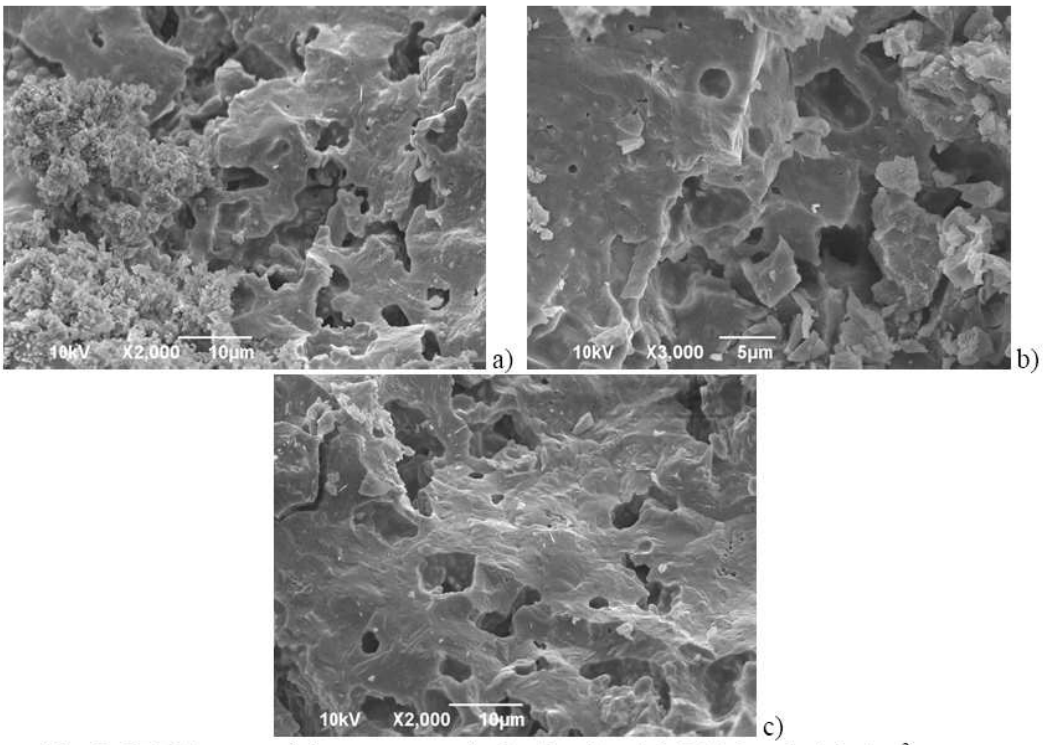

Fig. 3. SEM images of the compacts obtained under a) 0.5, b) 3 and c) 6 t/cm^2 pressure, sintered at 1350°C for 4h.

The absence of the small-grain structure in the samples compacted at pressures higher than 2tcm^{-2} indicates that this pressure is the critical pressure that enables better contacts between particles. Fig. 3. c) shows a stable structure with large surfaces and a closed porosity, typical of the final sintering stage, which is the obvious effect of the pressure applied prior to the sintering process. Higher pressures allow for a great number of contacts between particles, leading to more compact samples without the small-grain structure.

Fig. 4. shows the XRD patterns of the samples pressed under a) 0.5 tcm^{-2} and b) 6 tcm^{-2}, both sintered at 1350°C for four hours. The obtained peaks were identified using JCPDS cards (084-1220 for cordierite, 074-2220 for $Mg(OH)_2$, 083-2241 for TiO_2 rutile, 074-0201 for SiO_2, 035-0310 for $(MgAl)SiO_3$). The XRD pattern shown in Fig. 4. a) indicates the existence of a cordierite phase along with some amount of un-reacted starting components, such as SiO_2 and $Mg(OH)_2$. The presence of a rutile phase has been expected, because it was added not with the idea of incorporating it into the cordierite crystal lattice but with the intention to influence the mechanical and electrical properties. Accompanied with the sintering process, the pressure of 6tcm^{-2} yielded different phase compositions, as shown in Fig. 4. b). Apart from cordierite, as the major phase, no starting components (except TiO_2-rutile) have been detected. However, a $(MgAl)SiO_3$ phase is observed as a result of a reaction between the starting components, $Mg(OH)_2$ and SiO_2.

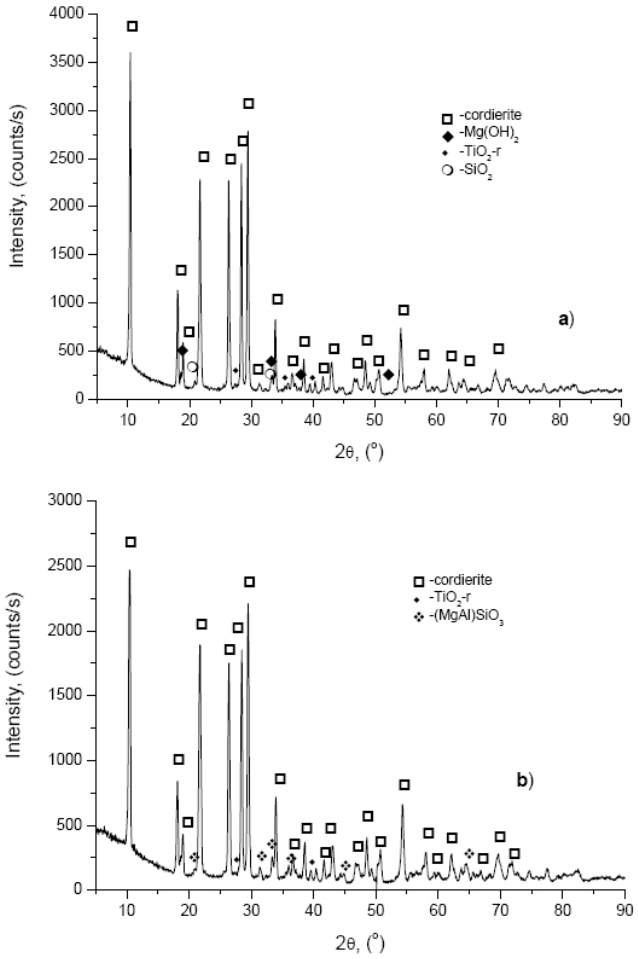

Fig. 4. XRD patterns of the samples compacted at a) 0.5 and b) 6t/cm^2 pressure, sintered at 1350°C for 4h.

The density after the sintering process at 1350ºC for four hours, as well as with the electrical properties of cordierite ceramics are presented in Tab. II.

Tab. II Density and electrical properties of cordierite after sintering at 1350ºC for four hours.

P (tcm^{-2})	C (pF)	tgδ	R (Ω)	ρ (gcm^{-3})	TG (%)	ε_r
0.5	1.89	0.009	$2\cdot10^{13}$	2.041	66.31	14.16
1	1.79	0.009	$3\cdot10^{13}$	2.075	67.41	13.21
2	1.81	0.010	$2\cdot10^{13}$	2.119	68.83	12.75
3	2.23	0.008	$3\cdot10^{13}$	2.154	69.98	15.21
4	2.10	0.008	$2\cdot10^{13}$	2.175	70.66	13.86
5	2.09	0.008	$3\cdot10^{13}$	2.192	71.21	13.53
6	2.09	0.007	$1\cdot10^{12}$	2.214	71.91	13.31

The electrical measurements are in a great accordance with the results presented earlier in this paper. It is obvious that they vary with the applied pressure. Two areas are visible: the first between 0.5 and 2tcm^{-2}, and the second between 3 and 6tcm^{-2} (parts I and II in Fig. 1). The values of the relative dielectric constant ε_r are increased, compared to the normal value for cordierite ceramics, due to the addition of TiO_2 and they vary in the interval from 13 to 15. Although the ε_r value is increased, it is still in the acceptable dielectric range.

4. Conclusions

The results of this study show that the applied pressure has an impact on the final characteristics of the sintered material:

- The density values of green bodies increase with the greater pressure applied and the greatest density is achieved after the compaction process at 6tcm^{-2}. Two stages are visible and the interval is between 2 and 3tcm^{-2}, indicating that powder particles are exposed to the agency of different mechanisms.
- The SEM micrographs clearly indicate a completely different microstructure: an open porosity and defined small-grain areas are observed in the powders pressed under lower pressures. With increased pressure values, a closed porosity and more homogeneous microstructures are obtained.
- According to the results presented in this study, the XRD analysis has shown a different phase composition in the sintered samples pressed under two limit pressures. The cordierite phase is the dominant phase; the starting components are present in the sample pressed under 0.5tcm^{-2}, whereas they were completely used in the reaction yielding a new phase in the sample pressed under 6tcm^{-2}.
- The final electrical properties are in great agreement with the presented results. The values of the relative dielectric constant show that the pressure of 2tcm^{-2} yields the results closest to the expected results; they are also consistent with standard demands related to the applicability of cordierite ceramics.

Based upon these results, we recommend compaction between 2 and 3tcm^{-2} as a phase preceding the sintering process because it ensures the most favorable phase composition, microstructure and electrical properties for this ceramic material.

5. References

1. A. I. Kingon, R. F. Davis, Engineer Materials Handbook, Vol. 2. “Ceramics” edited by S. J. Schneider, Jr., ASM International Metals Park, OH, p. 1191.
2. N. Obradovic, N. Djordjevic, S. Filipovic, N. Nikolic, D. Kosanovic, M. Mitric, S. Markovic, V. Pavlovic, Powder Technology 218 (2012) 157-161.
3. V.J. Powers, C.H. Drummond, Ceram. Eng. Sci. Proc. 7 (1986) 969.
4. I. Warsworth, R. Stevens, J. Eur. Ceram. Soc. 9 (1992) 153.
5. M. Pinero, M. Atik, J. Zarzycki, J. Non-Cryst. Solids 147 –148 (1992) 1523.
6. D. Kervadec, M. Coster, J.L. Chermant, Mater. Res. Bull 27 (1992) 967.
7. N. Clausen, G. Petzow, J. Phys. (Paris), 47 (1986) 693.
8. R. R. Tumala, J. Am. Ceram. Soc. 74 (1991) 895.
9. S. H. Knickerbocker, A. H.Kumar, L. W. Herron Am. Ceram. Soc. Bull. 72 (1993) 90.
10. N. Djordjevic, N. Obradovic, S. Filipovic, J. Zivojinovic, M. Mitric, S. Markovic, Tehnika – Novi materijali 21 (2012) 3, 329.

11. N. Đorđević, M.M. Ristić, Lj. Pavlović, M. Lazić, J. Stojanović, TEOTES, IV konferencija "Teorija i tehnologija sinterovanja" (2001) 25.
12. J. S. Reed, Introduction to the Principles of Ceramic Processing, Wiley, New York (1988) 158.
13. G. L. Messing, C. J. Markhoff, L. G. McCoy, J. Am. Ceram. Soc., 61 (1982) 857.
14. I. Shapiro, Adv. Powder Metall. Part. Mater., 3 (1994) 41.
15. J. K. Beddow, Particulate Science and Technology, Chemical Publishing Co.,Inc. New York, (1980), 285.
16. R. M. German, Particle Packing Characteristics, Metal Powder Industries Federation, Princeton, New Jersey, (1989) 59.
17. R. Panelli, F. A. Filho, Powder Tech., 114 (2001) 255.
18. N. Obradovic, S. Stevanovic, M. Mitric, M. V. Nikolic, M. M. Ristic, Science of Sintering, 39 (2007) 241.
19. A. R. Cooper, L. E. Eaton, J. Amer. Ceram. Soc., 45 (1962) 97.

***Садржај**: Обзиром на својства, кордијерит, $2MgO{\cdot}2Al_2O_3{\cdot}5SiO_2$, је високо температурски керамички материјал од великог интереса за научнике. Почетна смеша са додатком 5,00 масених % TiO_2 је активирана у високо енергетском млину, 10 минута. Притисак пресовања кје био у интервалу од 0,5 до 6 tcm^{-2} (49–588 MPa). Извршено је синтеровање испресака на 1350 °C током 4 сата у атмосфери ваздуха. Фазни састав активираних и синтерованих узорака извршен је помоћу рендгенске дифракције. Скенирајућом електронском микроскопијом анализиране су микроструктуре. Аутори су испитивали утицај притиска пресовања на синтеровање и електрична својства кордијерита.*

***Кључне речи:** механичка активација, густина, XRD, SEM, електрична својства, кордијерит.*

РЕПУБЛИКА СРБИЈА

ФИЗИЧКИ ФАКУЛТЕТ
УНИВЕРЗИТЕТА У БЕОГРАДУ

ДИПЛОМА

О СТЕЧЕНОМ ВИСОКОМ ОБРАЗОВАЊУ

Пелеш Предрага Адриана

РОЂЕН-А 1-VIII-1984. ГОДИНЕ У БЕОГРАДУ, САВСКИ ВЕНАЦ СРБИЈА, УПИСАН-А 2003/2004. ГОДИНЕ, А ДАНА 23. ДЕЦЕМБРА 2011. ГОДИНЕ, ЗАВРШИО-ЛА ЈЕ СТУДИЈЕ НА ФИЗИЧКОМ ФАКУЛТЕТУ УНИВЕРЗИТЕТА У БЕОГРАДУ, НА СТУДИЈСКОЈ ГРУПИ ФИЗИКА СА ОПШТИМ УСПЕХОМ 8,20 (ОСАМ И 20/100) У ТОКУ СТУДИЈА И ОЦЕНОМ 10 (ДЕСЕТ) НА ДИПЛОМСКОМ ИСПИТУ.

НА ОСНОВУ ТОГА ИЗДАЈЕ МУ-ЈОЈ СЕ ОВА ДИПЛОМА О СТЕЧЕНОМ ВИСОКОМ ОБРАЗОВАЊУ И СТРУЧНОМ НАЗИВУ

ДИПЛОМИРАНИ ФИЗИЧАР ЗА ПРИМЕЊЕНУ ФИЗИКУ И ИНФОРМАТИКУ

РЕДНИ БРОЈ ИЗ ЕВИДЕНЦИЈЕ О ИЗДАТИМ ДИПЛОМАМА 2120/2011

У БЕОГРАДУ, 27. ДЕЦЕМБРА 2011. ГОДИНЕ

ДЕКАН
ПРОФ. ДР Љубиша Бековић

РЕКТОР
ПРОФ. ДР Бранко Ковачевић

Република Србија
Универзитет у Београду
Физички факултет
Д.Бр.2011/8035
Датум: 19.11.2015. године

На основу члана 161 Закона о општем управном поступку и службене евиденције издаје се

УВЕРЕЊЕ

Пелеш (Предраг) Адриана, бр. индекса 2011/8035, рођена 01.08.1984. године, Београд, Београд-Савски Венац, Република Србија, уписана школске 2015/2016. године, у статусу: самофинансирање; тип студија: докторске академске студије; студијски програм: Физика.

Према Статуту факултета студије трају (број година): три.
Рок за завршетак студија: у двоструком трајању студија.

Ово се уверење може употребити за регулисање војне обавезе, издавање визе, права на дечији додатак, породичне пензије, инвалидског додатка, добијања здравствене књижице, легитимације за повлашћену вожњу и стипендије.

Овлашћено лице факултета

Научно веће ИТН САНУ

Деловодни број 373/2
Датум 11.10.2013.

На основу чланова 59, 70 и 82 Закона о научноистраживачкој делатности (Службени гласник Републике Србије бр. 110/05, 50/06 – исправка и 18/2010 – исправка), чланом 22 Статута Института техничких наука САНУ, чланом 45 Пословника о раду Научног већа ИТН САНУ и Правилником о утврђивању услова и предлога за стицање звања истраживач сарадник и избор у звање истраживач сарадник ИТН САНУ, на седници Научног већа одржаној 11.10.2013. године, донета је

ОДЛУКА
О СТИЦАЊУ ИСТРАЖИВАЧКОГ ЗВАЊА

Адриана Пелеш, дипломирани физичар

стиче истраживачко звање

истраживач сарадник

Образложење

Адриана Пелеш, дипломирани физичар, запослена на радном месту истраживача приправника у Институту техничких наука САНУ, покренула је 19.08.2013. године поступак за избор у истраживачко звање истраживач сарадник. На седници Научног већа од 23.08.2013. године је формирана Комисија за избор именоване у истраживачко звање, која је 03.09.2013. године поднела извештај о избору и који је стављен на увид јавности у електронском облику на вебстраници Научног већа и у принтаном облику у Секретаријату Института.

На основу овог извештаја Комисије и приложеног изборног материјала, утврђено је да Адриана Пелеш испуњава све услове из члана 70 Закона о научноистраживачкој делатности за стицање истраживачког звања истраживач сарадник, те је Научно веће једногласно одлучило као у диспозитиву одлуке.

ИНСТИТУТ ТЕХНИЧКИХ НАУКА САНУ основан 1947.г

Председник Научног већа

Академик Зоран Ђурић

Кнез Михаилова 35/IV, П.Ф. 377, 11000 Београд, Србија
Тел.: 011 21 85 437, 26 36 994; Факс: 21 85 263, мејл: its@itn.sanu.ac.rs, http://www.itn.sanu.ac.rs
Текући рачун: 840-1613660-30, 840-1613666-12, ПИБ: 100039438, матични бр. 07011016